Journal of Controlled Release 339 (2021) 361–380

Contents lists available at ScienceDirect

Journal of Controlled Release

journal homepage: www.elsevier.com/locate/jconrel

Dissolving microneedle patches loaded with amphotericin B microparticles for localised and sustained intradermal delivery: Potential for enhanced treatment of cutaneous fungal infections

Ke Peng [a], Lalitkumar K. Vora [a], Ismaiel A. Tekko [a,b], Andi Dian Permana [c], Juan Domínguez-Robles [a], Delly Ramadon [d], Philip Chambers [a], Helen O. McCarthy [a], Eneko Larrañeta [a], Ryan F. Donnelly [a,*]

[a] School of Pharmacy, Medical Biology Centre, Queen's University Belfast, 97 Lisburn Road, Belfast BT9 7BL, United Kingdom
[b] Faculty of Pharmacy, Aleppo University, Aleppo, Syria
[c] Department of Pharmaceutics, Faculty of Pharmacy, Hasanuddin University, Makassar, Indonesia
[d] Faculty of Pharmacy, Universitas Indonesia, Depok, Indonesia

ARTICLE INFO

Keywords:
Dissolving microneedles
Intradermal delivery
Sustained release
Amphotericin B
Fungal infections

ABSTRACT

Fungal infections affect millions of people globally and are often unreceptive to conventional topical or oral preparations because of low drug bioavailability at the infection site, lack of sustained therapeutic effect, and the development of drug resistance. Amphotericin B (AmB) is one of the most potent antifungal agents. It is increasingly important since fungal co-infections associated with COVID-19 are frequently reported. AmB is only administered *via* injections (IV) and restricted to life-threatening infections due to its nephrotoxicity and administration-related side effects. In this work, we introduce, for the first time, dissolving microneedle patches (DMP) loaded with micronised particles of AmB to achieve localised and long-acting intradermal delivery of AmB for treatment of cutaneous fungal infections. AmB was pulverised with poly (vinyl alcohol) and poly (vinyl pyrrolidone) to form micronised particles-loaded gels, which were then cast into DMP moulds to form the tips. The mean particle size of AmB in AmB DMP tips after pulverisation was 1.67 ± 0.01 μm. This is an easy way to fabricate and load microparticles into DMP, as few steps are required, and no organic solvents are needed. AmB had no covalent chemical interaction with the excipients, but the crystallinity of AmB was reduced in the tips. AmB was completely released from the tips within 4 days *in vitro*. AmB DMP presented inhibition of *Candida albicans* (CA) and the killing rate of AmB DMP against CA biofilm inside porcine skin reached 100% within 24 h. AmB DMP were able to pierce excised neonatal porcine skin at an insertion depth of 301.34 ± 46.86 μm. *Ex vivo* dermatokinetic and drug deposition studies showed that AmB was mainly deposited in the dermis. An *in vivo* dermatokinetic study revealed that the area under curve ($AUC_{0\text{-}inf}$) values of AmB DMP and IV (Fungizone® bolus injection 1 mg/kg) groups were 8823.0 d•μg/g and 33.4 d•μg/g, respectively (264-fold higher). AmB remained at high levels (219.07 ± 102.81 μg/g or more) in the skin until 7 days after the application of AmB DMP. Pharmacokinetic and biodistribution studies showed that AmB concentration in plasma, kidney, liver, and spleen in the AmB DMP group was significantly lower than that in the IV group. Accordingly, this system addressed the systemic side effects of intravenous injection of AmB and localised the drug inside the skin for a week. This work establishes a novel, easy and effective method for long-acting and localised intradermal drug delivery.

1. Introduction

Fungal infections are increasingly significant clinical issues across the globe. Almost a billion people are estimated to suffer from skin, nail or hair fungal infections and over 150 million people have serious fungal diseases that are fatal or greatly impact the quality of life [1]. The pandemic coronavirus disease 2019 (COVID-19) has necessitated the extensive use of systemic glucocorticoids, which heightens the risk of

* Corresponding author.
E-mail address: R.Donnelly@qub.ac.uk (R.F. Donnelly).

https://doi.org/10.1016/j.jconrel.2021.10.001
Received 25 June 2021; Received in revised form 23 September 2021; Accepted 3 October 2021
Available online 5 October 2021

opportunistic fungal infections in patients [2]. It has been reported that COVID-19 patients have a higher probability of suffering from invasive mycoses, including those caused by *Candida*, *Aspergillosis* and *Mucormycosis* [3,4].

The skin surface is the most common site for fungal infections, as it provides warm temperature and moist, ideal conditions for fungal growth [5,6]. Cutaneous fungal infections are common throughout the world, with a great prevalence (20–25% of the global population) [7]. As the most common form of fungal diseases, they lead to a large number of visits to dermatologists [8]. Cutaneous fungal infections can become contagious, severe, and invasive if not managed properly, especially in the immunosuppressed population [9]. Management of cutaneous fungal infections generally requires medication. Topical antifungal therapy is often effective in treating superficial fungal infections. However, after fungi infect the skin, they subsequently migrate through the *stratum corneum* (SC) to deeper tissues to avoid being shed from the skin surface by desquamation [6]. Topical antifungal therapies are insufficient for eradicating these infections because of poor drug penetration across the SC [10,11]. Even though the treatment of cutaneous fungal infections favours local delivery, which concentrates a greater amount of the drug on the site of infections and causes the least systemic toxicity, systemic antifungal therapies such as oral antifungals are the treatment of choice under deep-seated situations.

Antifungal agents include orally available azoles, polyene antibiotics, antimetabolites and microtubule inhibitors. Amongst all the therapies for fungal infections, the polyene amphotericin B (AmB) is one of the oldest yet most effective antifungal agents [12]. Despite its high toxicity, AmB remains the drug of choice in the clinic because of its broad spectrum of activity and rare incidence of clinical resistance, which give it great advantages over the azole class of antifungal agents [13]. It is the drug of choice in the treatment of infections caused by *Candida, Aspergillosis* and *Mucormycosis* [14,15]. Despite the versatility and importance of AmB in managing fungal infections, AmB is only used in very serious fungal infections [16]. The current clinical use of AmB is primarily restricted by its dose-related nephrotoxicity and infusion-related adverse reactions, including fever, chills or rigours, vomiting and headache [17]. Indeed, delivering such a drug directly to the site of action in the skin has several advantages, including sparing a high proportion of the systemically administered dose and reducing the unnecessary systemic AmB exposure, thus avoiding/reducing its systemic toxicity [18].

Intradermal drug delivery, which is defined as bypassing the outermost layer of the skin, the SC, using a suitable device and depositing the drug in the underlying viable skin layers, the epidermis, and dermis, is an attractive alternative drug delivery approach employed to overcome certain drug administration challenges [19–21]. However, intradermal delivery of AmB is largely constricted by the barrier of the SC. Molecules able to permeate the SC generally possess a low molecular weight (MW < 500 Da), balanced lipophilicity (log $P = 1$–3), and a measurable solubility both in oil and water [22]. AmB with a high molecular weight of 924 Da and a very poor aqueous solubility profile, unfortunately, but predictably, has difficulty in cutaneous permeation. Indeed, the limited permeation of AmB through the SC has been well documented in the literature, and, until now, few AmB topical formulations have been approved by the Food and Drug Administration (FDA) [23]. For example, a topical lipid gel formulation for AmB named Amfy® gel from Intas Pharmaceuticals Ltd. is available in India. This gel was used as a reference in the literature and was found to deliver little AmB through the skin [24]. Anfoleish®, a cream containing 3% AmB, failed a clinical phase II study of Colombian cutaneous leishmaniasis patients due to its poor efficacy [25].

Microneedle patches provide a promising platform for enhancing intradermal delivery of "difficult to deliver" therapies. Microneedle patches are minimally invasive devices that comprise multiple micron-scale projections on a patch [26–29]. The sharp and tiny projections can bypass the SC and deliver the drug into the viable layers of the skin without touching the nerves deeper in the skin [30]. The use of microneedle patches could be a promising alternative to conventional methods in the delivery of AmB [10,31]. Various materials have been explored to fabricate microneedle patches. Of them, microneedle patches made from dissolving polymers (dissolving microneedle patches, DMP) have great advantages, as they are convenient to use, leave no sharp hazard and are capable of delivering high drug doses [32].

This work explored the potential of DMP to deliver AmB intradermally to maximise its antifungal therapeutic effects while minimising systemic exposure and toxicities in treating cutaneous fungal infections. Various AmB DMP were formulated and characterised for their drug content, mechanical properties, insertion ability both *in vitro* and *ex vivo*, and their *ex vivo* intradermal delivery potential. A rationalised formulation was then studied for their particle size, *in vitro* release profiles and thermoanalysis. Antifungal tests were performed both *in vitro* and in an *ex vivo* fungal infection skin model. Moreover, the *ex vivo* dermatokinetic profiles were studied, followed by *ex vivo* drug distribution investigation and *in vivo* dermatokinetic studies. *In vivo* pharmacokinetic and biodistribution studies in mice were also performed to reveal the formulation's systemic absorption.

2. Material and methods

2.1. Materials

AmB was purchased from Cayman Chemical Company (Item No. 11636, Batch No. 0552510, purity specification ≥95%, Ann Arbor, MI, USA). Poly (vinyl alcohol) MW 9–10 kDa (PVA), and poly (vinyl alcohol) MW 31–50 kDa (PVA—H) were both purchased from Sigma-Aldrich (Poole, Dorset, UK). Plasdone™ K-29/32 (poly(vinylpyrrolidone), PVP), (MW58 kDa) was donated by Ashland (Kidderminster, UK). Ethylenediaminetetraacetic acid disodium salt dehydrate (Na_2EDTA), dodecyl sodium sulfate (SLS), HPLC-grade methanol, acetonitrile, and tetrahydrofuran were also supplied by Sigma-Aldrich (Poole, Dorset, UK). Dimethyl sulfoxide (DMSO) was provided by VWR International Limited, Leicestershire, UK. Phosphate buffered saline (PBS) pH 7.4 tablets were acquired from Oxoid Limited, Hampshire, UK. Fungizone® (50 mg powder for sterile concentration) was manufactured by Bristol-Myers Squibb, Princeton, NJ, USA, and ordered from Lockview Pharmacy Stranmillis, Belfast, UK. Micropore® tape was supplied by 3 M UK Plc, Bracknell, Berkshire, UK. An occlusive dressing layer (Tegaderm™) was obtained from 3 M, St Paul, Minnesota, USA. Parafilm® M was purchased from Bemis Company, Neenah, Wisconsin, USA. Heparin sodium was acquired by Wockhardt® Ltd., Wrexham, UK. Purified water was obtained using a water purification system, Elga PURELAB DV 25, Veolia Water Systems, Ireland. All other chemicals used were of analytical reagent grade.

2.2. Fabrication of AmB DMP

To minimise drug wastage, AmB was only loaded in the DMP tips. Formulations with a range of drug contents were prepared for casting the drug-containing tips as per Table 1. Dissolvable polymers, PVP and

Table 1
Formulation compositions for casting tips of AmB DMP.

Formulation code	Composition% (w/w)			
	AmB	PVP	PVA	Water
F1	20	10	10	60
F2	30	10	10	50
F3	40	10	10	40
F4	50	10	10	30
F5	40	20	0	40
F6	40	0	20	40

PVA, were added to form the drug-containing tips of AmB DMP. The drug proportion was increased until the formulation was unable to be further homogenised. The formulations are further detailed in Table 1.

The process of microneedle fabrication involved two-step casting as illustrated in Fig. 1. Briefly, the formulations were weighted according to the composition of Table 1 and then homogenised using a Speedmixer™, DAC 150 FVZ-K (Synergy Devices Ltd., London, UK) at 3000 rpm for 5 min to form the drug gels. The resultant gels were immediately cast into the silicone microneedle moulds (16 × 16 needles arranged on a 0.50 cm^2 area with 850 μm needle height [600 μm pyramidal tip, 250 μm base column], 300 μm column width, and 100 μm interspacing). The moulds were placed inside a pressure chamber and a positive pressure of 5 bar was applied for 3 min. The excess gel was scraped from the moulds using a spatula, and the moulds were placed back inside the pressure chamber at a positive pressure of 5 bar for 30 min. Following this, an aqueous drug free-gel consisting of PVP (20%, *w*/w) and PVA-H (15%, w/w) was poured onto the moulds and centrifuged at 3745 ×*g* for 15 min. The drug-free gel cast in the moulds was allowed to dry at 37 °C for 48 h to form the baseplate of the microneedle patches.

2.3. Characterisation of AmB DMP

2.3.1. Drug content analysis

The amount of AmB loaded in each AmB DMP was determined by extracting the drug-containing microneedle tips with 1 mL of DMSO (n = 6). After vortexing the samples for 15 min to fully extract the drug, centrifugation at 16160 ×*g* for 15 min was employed. An aliquot of 10 μL of the clear supernatant was collected and diluted with 990 μL of methanol. The diluted samples were then analysed using a validated reversed-phase high-performance liquid chromatography (HPLC) method with ultraviolet detection, as described in Section 2.8.

2.3.2. Compression test and in vitro insertion behaviour

A compression test of AmB DMP was performed using a TA-XT2 Texture Analyser (Stable Microsystems, Haslemere, UK) as an initial mechanical characterisation, as previously described [33,34]. Briefly, an AmB DMP was attached to the moveable probe of the Texture Analyser and was then pressed against a flat aluminium block at a 32 N force for 30 s. The pre- and post-test speeds were both set at 0.50 mm/s and the trigger force was 0.049 N. Tips of AmB DMP were imaged and analysed using a Leica EZ4W digital microscope (Leica, Wetzlar, Germany) before and after the compression load. The percentage of the change in the height of the needles after compression was calculated (n = 100).

Parafilm M® (PF) was used as a simulated skin model for *in vitro* insertion experiments, as previously described [35]. AmB DMP were applied against an eight-sheet PF laminate using the Texture Analyser with a speed of 0.50 mm/s and an exerted force of 32 N per patch (0.125 N per needle) for 30 s. The force has been demonstrated to be the mean force exerted by a person when self-administering a microneedle patch [35]. The patch was then carefully removed from the PF, the PF layers were unfolded, and the number of holes created in each layer was counted using the digital microscope. The percentage of holes created *versus* the depth of PF layers was plotted. The thickness of each PF layer was previously reported to be 126 ± 7 μm [36] (n = 3).

2.3.3. Ex vivo drug deposition in the skin

An *ex vivo* skin deposition study of the AmB DMP was conducted using full-thickness neonatal porcine skin obtained from stillborn piglets as a surrogate of human skin due to their remarkable similarities in general structure and physical properties [37]. The AmB DMP were chosen considering the results obtained from the drug content analysis and the mechanical characterisation. Before starting the study, the skin samples were shaved and hydrated in PBS (pH 7.4) for 1 h. The skin was then fixed on the donor compartment of static vertical glass Franz diffusion cells, as previously documented [38]. The AmB DMP were applied with manual force for 30 s and then a cylindrical stainless-steel weight (12 g) was placed on top of the patch to keep it in place. For this study, freeze-dried F3 formulation gel was used as a control, which contained 3 mg of AmB, 0.75 mg of PVP, and 0.75 mg of PVA. It was spread on top of the skin in the donor compartment and mixed with 1 mL of deionised water. The receptor compartment of the Franz cell was filled with 12 mL of the degassed PBS containing 1% *w/v* SLS and maintained at 37 ± 1 °C. The receptor medium was continuously stirred using a magnetic stirrer. The diffusion cells were equilibrated for 30 min and then the donor compartment was mounted on the Franz diffusion cell. After 24 h application, tissue samples were cleaned to remove the drug on the skin surface and punch biopsy (8 mm size) was used to remove parts of samples at the locations where the patches or the formulation gel had been placed. The skin sample was then homogenised with 1 mL of DMSO at 50 Hz using a Tissue Lyser LT (Qiagen, Ltd., Manchester, UK) for 10 min and centrifuged at 16,160 ×*g* for 20 min. The supernatant was collected, diluted, and then analysed using HPLC (n = 5).

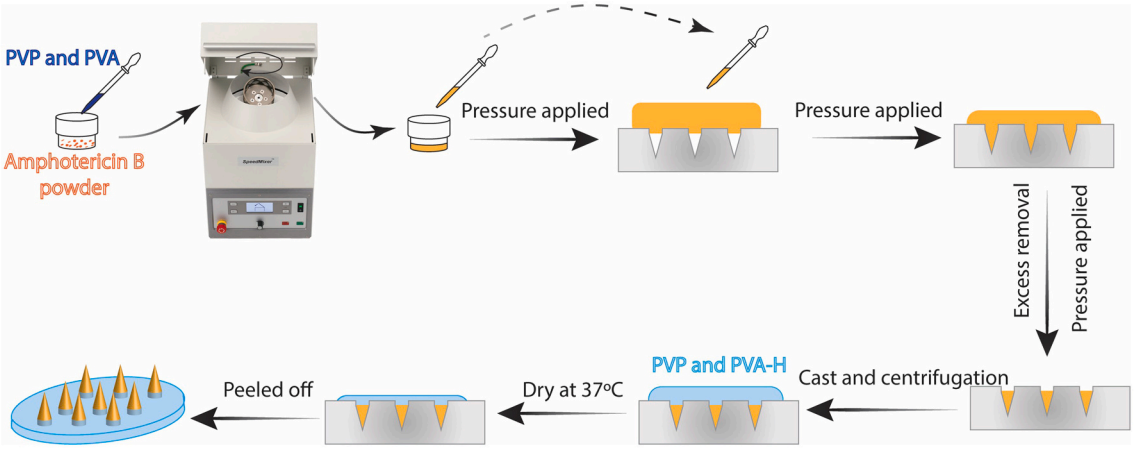

Fig. 1. Schematic representation of the fabrication process of AmB DMP. The formulations were placed in the Speedmixer™ container and mixed using the Speedmixer™ at 3000 rpm for 5 min. The formulated gel was added to the microneedle moulds. A pressure of 5 bar for 3 min was immediately applied to fill the cavities of the microneedle moulds. The excess drug gel was removed by a spatula and the moulds were placed inside the pressure chamber using 5 bar for 30 min. The tips inside the moulds were then dried overnight. An aqueous gel of PVP and PVA-H was poured on the moulds and centrifuged at 3745 ×*g* for 15 min. The moulds were dried at 37 °C for 48 h. AmB DMP were peeled off from the moulds.

2.4. Characterisation of AmB DMP tips

2.4.1. Particle size measurements and morphology

The particle size distribution (PSD) of dry AmB DMP tips and AmB powder were determined by static light scattering using a Helos particle size analyser (Sympatec, GmbH, Clausthal-Zellerfeld, Germany). AmB DMP tips were collected and suspended in deionised water in a 50 mL glass cuvette to a suitable optical density and stirred with a magnetic bar at 1000 rpm. AmB powder was suspended in deionised water and tested in the same way. A short period of sonication (60 s) at a power of 60 W was applied by an 8.5 mm diameter ultrasound tip before sizing. An R2 lens was used, allowing measurements in the range of 0.25–87.5 μm. The particle sizes d_{10}, d_{50} and d_{90} (*i.e.*, the size in microns at which 10%, 50% and 90% of the particles are smaller) were recorded. All measurements were carried out in quadruplicate.

The tips of AmB DMP were examined using a digital stereo microscope (VHX-1020, Keyence, Osaka, Japan). Some tips of AmB DMP were slightly crushed in an attempt to investigate the surface and cross-section surface morphology and a scanning electron microscope (SEM) with a Quanta FEG 250 (FEI, Hillsboro, OR, USA) was used at an acceleration voltage of 10–20 kV under high vacuum pressure (8×10^{-5} mbar).

2.4.2. Thermo-gravimetric analysis

AmB powder, a physical mixture of AmB, PVA, and PVP (4/1/1, *w*/w/w) and the dry powder cast from F3 formulation were separately analysed using a TGA Q500 (TA instruments, Bellingham, USA) with a heating rate of 20 °C/min until 400 °C under 40 mL/min N_2 flow.

2.4.3. Differential scanning calorimetry analysis (DSC)

DSC thermal analysis of samples, *i.e.* AmB powder, a physical mixture of AmB, PVA, and PVP (4/1/1, *w*/w/w) and the dry powder cast from F3 formulation, was performed on a DSC Q100 (TA instruments, Bellingham, USA). Briefly, samples (5–10 mg) were analysed from 0 °C to 180 °C at a scanning rate of 20 °C/min under a N_2 atmosphere at a flow rate of 50 mL/min.

2.4.4. Powder X-ray diffraction studies (PXRD)

The crystallinity of AmB powder, physical mixture (AmB, PVA, and PVP, 4/1/1, w/w/w), and the dry powder cast from F3 formulation was analysed using (wide angle) PXRD on a MiniFlex II Desktop Powder X-ray Diffractometer (Rigaku Corporation, Kent, England) with Cu Kα radiation (30 kV) at a current of 15 mA. Samples were pulverised before analysis. The required amount of sample was placed onto a glass plate which was then mounted on the sample holder. X-ray diffractogram was scanned in the angular range (2θ) varying from 5° to 40° using a step scan mode with a step width of 0.02° and a counting time of 2 s/step.

2.4.5. Fourier transform infrared spectroscopy studies (FTIR)

Intra/intermolecular interactions between the drug and polymers were characterised by attenuated total reflection-Fourier transform infrared spectroscopy (ATR-FTIR). All samples were scanned from 4000 cm^{-1} to 600 cm^{-1}, with 4.0 cm^{-1} resolution and 64 scans per spectrum using a Spectrum Two FTIR Spectrometer (Perkin Elmer, Waltham, MA, USA).

2.4.6. In vitro release study

The release of AmB from AmB DMP tips was studied using 15 mL of PBS (pH 7.4) containing 1% *w/v* SLS as the release medium. The dry tips without the baseplate were collected. The experiment was conducted under exclusion from light using a thermal incubator at 40 rpm and 37 ± 1 °C. Samples (1 mL) were taken at predetermined time points (1, 2, 3 and 4 days) and immediately replaced with fresh release medium. In comparison, 3 mg of AmB powder was added to 15 mL of PBS containing 1% w/v SLS ($n = 5$). The samples of AmB powder were taken in the same way as for the AmB DMP tips.

2.5. Antifungal examination of AmB DMP

2.5.1. Disk diffusion test

Antifungal activity of F3 AmB DMP, blank DMP (without AmB) and paper discs containing 3 mg of AmB against *Candida albicans* NCYC 610 (CA) was determined using a modified radial diffusion assay [39–42]. Briefly, the fungal culture was freshly prepared and demonstrated a viable colony-forming units (CFU) concentration of 6×10^6 CFU/mL. The culture (1 mL) was added to 5 mL of a soft Sabouraud dextrose agar and the mixture was vortexed and then poured on the surface of a Sabouraud dextrose agar (SDA) plate. After cooling down and solidifying the culture, AmB paper discs, F3 AmB DMP and blank DMP were placed in the centre of the plate and pressed gently with sterile forceps. After incubation at 37 °C for 24 h, the zone of inhibition around the patches or discs was measured. The whole process was conducted under aseptic conditions and untreated inoculated plates were used as a control ($n = 5$).

2.5.2. Antimicrobial assay in an ex vivo infection model on porcine skin

The antimicrobial activity was studied using a method previously described with slight modifications [43]. Full-thickness neonatal porcine skin was shaved, cut into a circular shape with a diameter of 30 mm, and soaked with 70% *v*/v ethanol for 30 min. An aliquot of 100 μL CA suspension (6×10^6 CFU/mL) was inoculated by subcutaneously injecting into the skin and spread homogeneously. The inoculated skin was kept in SDA plates for 3 days at 37 °C to culture the inoculum. After 3 days' culture, the inoculated skin was fixed in a Franz diffusion donor cell (15 mm orifice diameter). AmB DMP and blank DMP were applied to the inoculated skin using manual force for 30 s and a 12-g weight was placed on top of it. The treatment of infected skin models was performed for 24 h using a modified Franz diffusion cell setup. In brief, the infected skin samples were glued with cyanoacrylate adhesive (Loctite, Dublin, Ireland) to the donor compartments of the Franz diffusion cells, which were then mounted onto the receptor compartments of the Franz cells and affixed using clamps. The receiver compartments were filled with degassed PBS containing 1% *w/v* SLS with a stirring speed of 600 rpm. The system was kept at 37 ± 1 °C using a circulating water jacket. After application of the patches for 24 h, the infected skin samples were collected and placed into a 2 mL Eppendorf tube with 1 mL of sterile PBS. Tissue Lyser LT was set at 50 Hz for 10 min to harvest all the fungi from the skin samples. The resultant fungal suspensions were analysed for viable counts. Inoculated skin samples without application of any DMP were used as a control. The fungicidal activity was evaluated by the reduction rate of fungal growth after the treatment ($n = 3$).

2.6. Ex vivo delivery of AmB from AmB DMP

2.6.1. Ex vivo dermatokinetic study

An *ex vivo* dermatokinetic study of the AmB DMP was performed using modified Franz diffusion cells. Full-thickness neonatal porcine skin was shaved and hydrated in PBS (pH 7.4) for at least 30 min and then carefully fixed with cyanoacrylate adhesive into vertical Franz diffusion cells. The AmB DMP were then inserted into the skin sample on top of the PF layers (to provide support without damaging the tips) for 30 s using gentle plunger pressure. A 12-g metal weight was placed on top of the patch to prevent extrusion from the skin. The Franz cell set-up was used as detailed in Section 2.3.3. At the time points of 0.25, 0.5, 0.75, 1, 2, 3, 4, 5, 6, and 24 h, the AmB DMP were removed, and the skin samples were cleaned three times with deionised water. The separation of epidermis from the dermis of the skin samples was achieved by heat-separation as it is a reliable method and widely-reported in the literature [44,45]. In brief, the skin samples were cut using a biopsy punch (8 mm size) and were then placed into a glass vial at 60 °C for 2–3 min. The epidermis layers were then separated manually from the dermis layers using a pair of sharp forceps. An aliquot of 0.4 mL DMSO was used to extract the drug inside epidermis layers, while 1 mL of DMSO was added

to extract the drug inside the dermis layers. The mixture was homogenised using a Tissue Lyser LT at 50 Hz for 5 min (for epidermis samples) or 20 min (for dermis samples). The resulting suspension was centrifuged at 16160 ×*g* for 6 min and the supernatants were collected, diluted 4 times using methanol, and analysed using HPLC. ($n = 4$).

To analyse the dermatokinetic profiles, PKSolver (China Pharmaceutical University, Nanjing, China) [38] was utilised with a one-compartmental open model after the construction of a curve consisting of drug concentration *versus* time. Several dermatokinetic parameters were observed, namely the maximum drug concentration (C_{max}), the time of maximum concentration (t_{max}), the area under the drug concentration-time curve from time zero ($t = 0$) to the last experimental time point ($t = 24$ h) (AUC), the mean half-life ($t_{1/2}$) and the mean residence time (MRT). Non-compartmental analysis was conducted where the one-compartmental open model was not applicable.

2.6.2. Ex vivo skin insertion performance of AmB DMP and drug distribution in the skin

To investigate the insertion depth AmB DMP reached in the skin, an EX1301, optical coherence tomography (OCT) microscope (Michelson Diagnostics Ltd., Kent, UK) and a Leica TCS SP8 MP multiphoton microscope (Leica Microsystems, Wetzlar, Germany) were used. The insertion depth of the tips of AmB DMP in the skin was visualised by OCT immediately after insertion and calculated using the imaging software ImageJ (National Institutes of Health, Bethesda, USA). A Leica TCS SP8 MP multiphoton microscope excited fluorescence upright microscope DM6000 CFS was utilised to visualise the drug inside the skin after the 24-h application of AmB DMP. Samples were excited using IR Mai Tai Ehp Deep See tunable from 690 nm to 1040 nm with a wavelength of 780 nm. Fluorescence emission was collected between 400 nm and 555 nm using internal HyD spectral detectors with 10×/ 0.4NA HC PL APO, PH1 dry objective lens. Images were acquired and analysed using Leica LAS-X software.

2.7. In vivo studies

2.7.1. Study design and drug administration procedures

In vivo studies were performed in compliance with the policy of the Federation of European Laboratory Animal Science Associations and the European Convention for the protection of vertebrate animals used for experimental and other scientific purposes, with the implementation of the principles of the 3Rs (replacement, reduction, and refinement). Approval was obtained from the Committee of the Biological Research Unit, Queen's University Belfast to conduct this study under the Project License PPL 2903 and Personal Licenses PIL1747 and 1892.

Female Balb/c mice aged 6–8 weeks with a weight of 18.86 ± 1.04 g were used in the study. The mice were allowed to acclimatise to laboratory conditions for at least 7 days before the experiment. The animals were separated into three cohorts (as depicted in Fig. 2): Cohort A ($n = 24$), where mice received the drug by intravenous (IV) injection, each mouse received a single dose of Fungizone® solution (1.0 mg/kg). In cohort B (n = 24), the mice received the drug by AmB DMP, each mouse receiving one patch of AmB DMP. Three mice were kept in the whole process of the study as a naïve control group ($n = 3$).

For mice that received the drug by AmB DMP, to prevent hair interference with DMP application, the hair on the back of the animals was removed using an electric clipper and hair removal cream for sensitive skin (Veet Health & Personal care, Berkshire, UK) while the mice were sedated using gas anaesthesia (2–4% isoflurane in oxygen). After 24 h (to allow full skin integrity recovery), the animals were anaesthetised again and a patch of AmB DMP was applied to the back of each mouse with firm finger pressure for 30 s. The AmB DMP were then secured in place using Microfoam™ surgical tape (3 M, Bracknell, UK) and then a non-occlusive adhesive film of Tegaderm™ (3 M, St Paul, Minnesota, USA). To further secure the AmB DMP in place, micropore surgical tape (3 M, St Paul, Minnesota, USA) was then gently wrapped around the back and abdomen of each animal. AmB DMP were applied on the animals for no longer than 24 h.

The mice in cohort A (IV group) were euthanized at the predetermined time points (0.25, 1, 4 and 24 h, and then at 2 and 4 days). The mice in cohort B (AmB DMP group) were also euthanized at

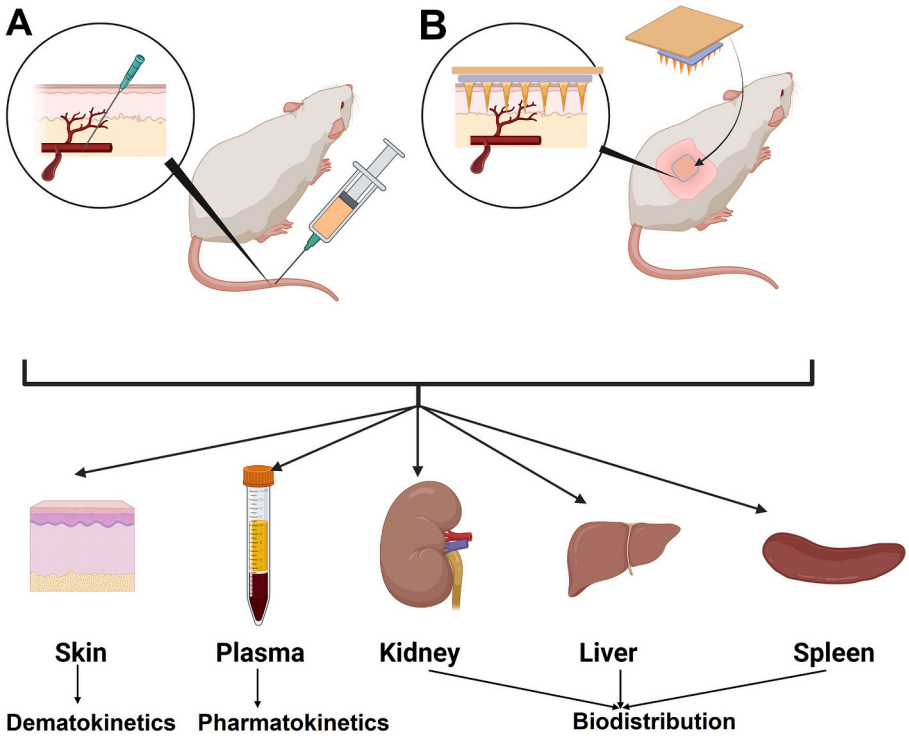

Fig. 2. Schematic representation showing the two treatment cohorts investigated in the *in vivo* experiment. (A) Bolus intravenous injection of 1.0 mg/kg of Fungizone®. (B) Intradermal application of AmB DMP to the shaved back of the mice. The dermatokinetics profiles were characterised based on the drug levels in the skin. The pharmacokinetic profiles were plotted using the drug levels in the plasma. The biodistribution profiles were presented using the drug levels in the kidneys, livers, and spleens for both cohorts.

predetermined time points (1, 4, 24 h and then at 2, 4, and 7 days). At each time point, blood was collected by cardiac puncture in heparin-containing Eppendorf tubes. Body organs, including skin, kidney, liver and spleen, were also harvested from each animal. In Cohort B (AmB DMP group), skin samples from the AmB DMP application sites and 2.0 ± 0.5 cm away from the AmB DMP application sites were collected.

2.7.2. Blood samples handling and processing

The blood obtained was processed using centrifugation at 3000 ×*g* for 10 min at 4 °C, after which the plasma was taken from the supernatant. AmB was extracted from the plasma using methanol added at a 2:1 ratio of methanol to plasma. Samples were vortexed and mixed for 1 min for complete drug extraction and protein precipitation. The mixture was stored at 4 °C for 1 h and then centrifuged at 16,160 ×*g* for 15 min at 4 °C. The supernatants were analysed by HPLC, as described in Section 2.8. The plasma concentrations of AmB were plotted as the pharmacokinetic profiles.

2.7.3. Organ samples handling and processing

The organ samples harvested from the animals were rinsed using PBS (pH 7.4) and then stored at −20 °C until processing. The skin and organ samples were homogenised in methanol at a ratio of 0.25 g (skin samples) or 1 g (organ samples) to 5 mL of methanol using a Tissue Lyser LT at 50 Hz for 15 min. Homogenates were vortexed at 1500 rpm for 1 h to allow complete drug extraction and then centrifuged at 16,160 ×*g* for 15 min. The drug levels of AmB in these tissues were determined using the supernatant and analysed by the validated HPLC method, as described in Section 2.8. The AmB concentrations in the skin samples *vs* time were plotted as the dermatokinetic profiles. The concentrations of AmB in the kidney, liver and spleen were plotted separately as indexes of biodistribution studies.

2.7.4. Calculation of dermatokinetic parameters, pharmacokinetic parameters

Non-compartmental model analysis was applied for the *in vivo* dermatokinetic and pharmacokinetic profiles using PK Solver [46]. The parameters calculated included the maximum drug concentration (C_{max}), The time of maximum concentration (T_{max}), the area under the drug concentration-time curve from time zero ($t = 0$) to the last experimental time point ($t = 96$ h for IV group, and $t = 168$ h for AmB DMP group) ($AUC_{0\text{-}t}$), the area under the drug concentration-time curve from time zero (t = 0) to infinity ($AUC_{0\text{-}inf}$), the mean half-life ($t_{1/2}$) and the mean residence time (MRT), where applicable.

2.8. Instrumentation and chromatographic condition for analytical method

Quantification of AmB in all samples was carried out using HPLC with an Agilent Technologies 1220 Infinity Compact LC Series with Agilent degasser, binary pump, auto standard injector and UV detector (Agilent Technologies UK Ltd., Stockport, UK). Separation was achieved by using a C18 Phenomenex SphereClone™ analytical column (150 mm × 4.60 mm internal diameter, 5 μm packing) with a flow rate of 1 mL/min. The mobile phase consisted of 35% *v*/v of 2.5 mM Na_2EDTA and 65% v/v of a mixture of methanol, acetonitrile and tetrahydrofuran (41:18:10, v/v/v). The analyses were performed using UV detection at 385 nm and the injection volume was 50 μL. The analyses were performed at 30 °C. The *in vitro* method was validated based on International Committee on Harmonisation (ICH) 2005 guidelines [47]. The *in vivo* method was validated according to EMEA guidelines [48].

2.9. Statistical analysis

All quantitative data were expressed as means ± standard deviation (SD) from triplicate measurements unless otherwise noted. Differences between three groups were assessed for significance using single-factor analysis of variance and differences between two groups were evaluated using Student's *t*-test. Statistical analysis was performed using Prism 7 (GraphPad Software, USA). Statistical significance was denoted by $p < 0.05$ in all cases.

3. Results and discussion

3.1. Fabrication and characterisation of AmB DMP

3.1.1. Fabrication

Various formulations for AmB DMP were prepared using aqueous blends of PVA and PVP as matrices. PVP and PVA were chosen because they are both safe [49,50], and can form mechanically strong DMP to deliver hydrophobic drugs, as demonstrated by several studies [18,51–54]. Furthermore, AmB and PVP complexes exhibited comparable antifungal effects to AmB with less toxicity [54].

The theoretical microneedle tip volume of the moulds was 11.52 mm^3. To maximise drug loading in the AmB DMP, first, the AmB concentration of the drug gels was increased from 20% *w*/w to 50% w/w to achieve the highest possible drug loading. By increasing the concentration of AmB, the drug gels became more viscous. As shown in Table 2, all formulations except F4 produced uniform and sharp needle arrays. Amongst all the AmB DMP, AmB (yellow) was located in the tips of the AmB DMP and the baseplate (transparent) contained only traces of AmB due to the manufacturing process. At a concentration of 50% *w*/w, the gel was too viscous to be spread on the moulds evenly. As a result, gels with AmB loading at 40% w/w (F3, F5, and F6) were chosen for further studies.

3.1.2. Drug content analysis

The drug content of all the formulated AmB DMP was analysed using a validated HPLC method and presented in Table 2. As estimated, drug content increased from 1.58 ± 0.17 mg to 2.80 ± 0.34 mg per patch with the increase of the concentration of AmB from 20% to 40% w/w. With the same concentration of AmB (40% *w*/w), the drug content was not significantly different when using different ratios of PVP and PVA (F3, F5, and F6, $p > 0.05$). The amount of the drug loaded in the system was much higher compared to a recently published paper on delivery of AmB using dissolvable microneedle patches, where the drug content was found to be 182 ± 4 μg per 22 × 22 microneedle array [55]. Peng et al. designed implantable microneedle systems to deliver AmB, where a patch of 11 × 11 microneedles was able to hold a maximum load of 160.0 ± 7.4 μg of AmB [31]. An inkjet-coated Gantrez® AN 169 microneedle patch was able to carry 10.4 μg of AmB. Its antifungal activity against *Candida parapsilosis* (ATCC 22019) in agar plates was comparable to that of a paper disk containing 10 μg of AmB [40]. Furthermore, coated poly(glycolic acid) microneedle patches were developed to deliver AmB topically. However, there was no report regarding the drug content of the device or the skin deposition. The agar diffusion assay result against CA was comparable to that of paper disks loaded with 10 μg of AmB [56]. The amount of the drug loaded in our systems was much higher compared to all previously published papers using microneedle technology to deliver AmB, indicating the potential of the current systems. This can be attributed to the relatively higher needle volume (11.52 mm^3) of the moulds we used to fabricate the patch [57].

3.1.3. Compression test and in vitro insertion behaviour

A compression test was conducted to evaluate the mechanical strength that DMP can withstand before they deform [58]. As presented in Fig. 3A, after a 32-N compression, the average height reduction rates of all the formulated AmB DMP were below 15%. Amongst all the groups, F3 AmB DMP displayed the lowest height reduction with a value of 9.89 ± 5.08%. A one-way analysis of variance elucidated the height reduction of F3 AmB DMP was significantly lower than that of F1 AmB DMP ($p < 0.001$) and F6 AmB DMP ($p < 0.001$). Needle height

Table 2
Formulation selected for the fabrication of AmB DMP and their morphology as well as the drug content of the patches ($n = 6$, means ± SD).

Code	Composition% (*w*/w)			Patch morphology	Drug content (mg/patch)
	AmB	PVP	PVA		
F1	20	10	10	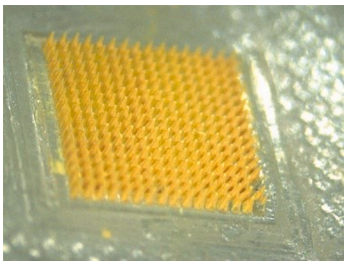	1.58 ± 0.17
F2	30	10	10	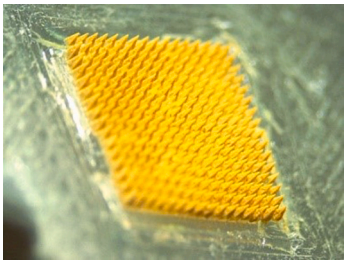	2.37 ± 0.46
F3	40	10	10	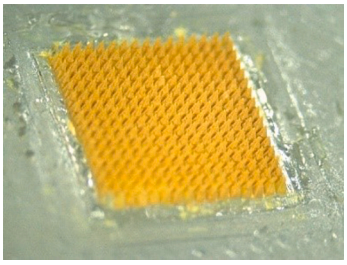	2.80 ± 0.34
F4[a]	50	10	10		–
F5	40	20	0	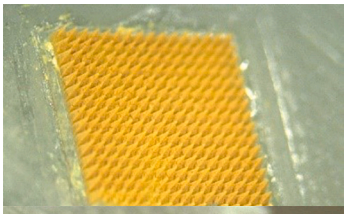	3.06 ± 0.64
F6	40	0	20	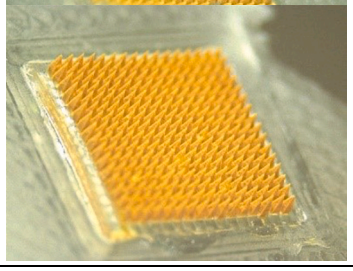	2.99 ± 0.21

[a] The F4 gel was too viscous to form uniform tips.

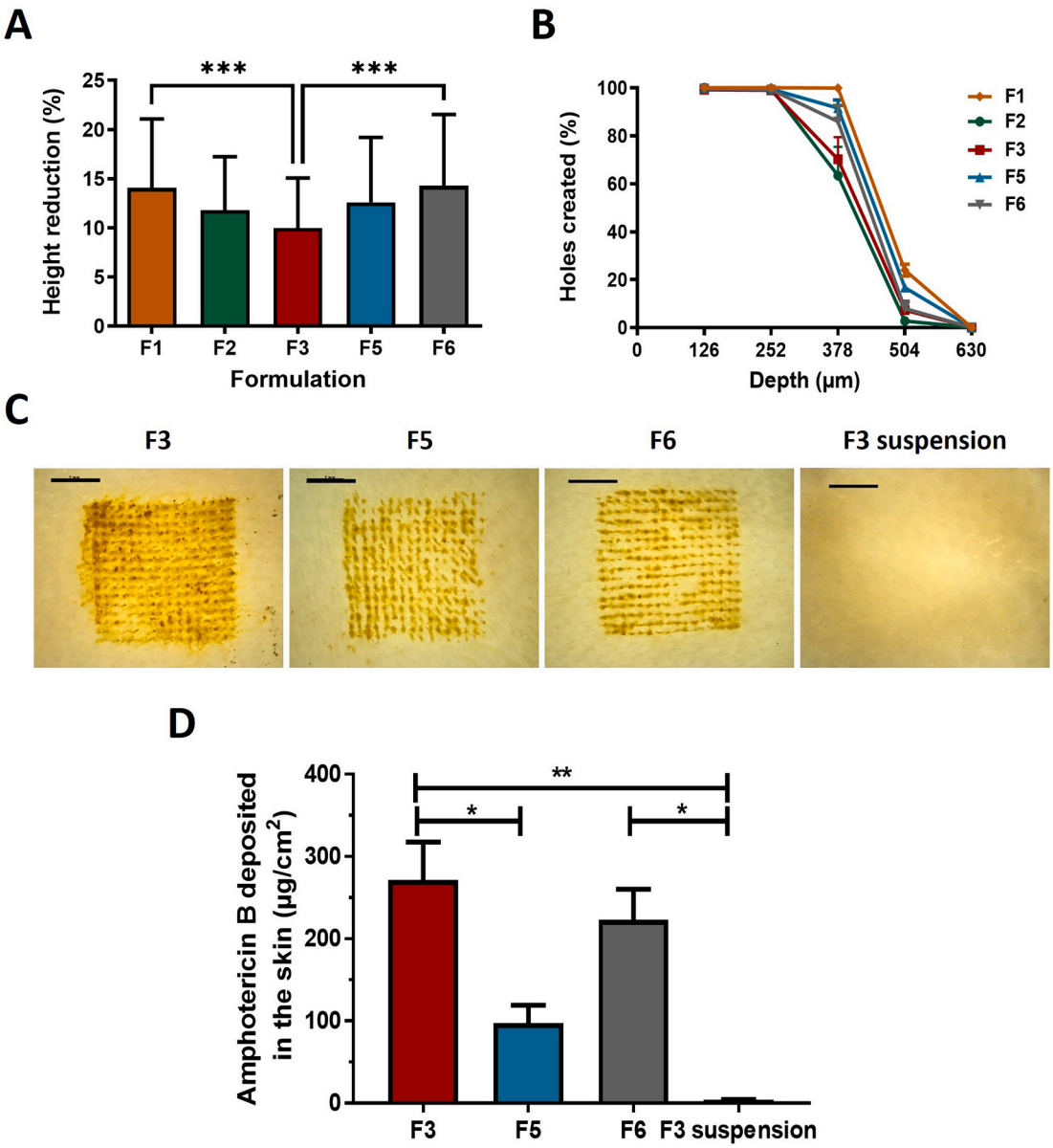

Fig. 3. AmB DMP characterisation. (A) Comparison of the percentage height reduction of AmB DMP formulations tested, observed following the application of a force of 32 N/array. (B) Percentage of holes created in each Parafilm M® layer following insertion of AmB DMP. (means + S.D., $n = 3$). (C) Representative skin deposition images after applying F3, F5, F6 AmB DMP and F3 suspension in the porcine skin for 24 h. (D) The skin deposition results of F3, F5, F6 AmB DMP and F3 suspension after 24-h application in the porcine skin. (means ± SD, $n = 4$; $^{*}p < 0.05$, $^{**}p < 0.01$, $^{***}p < 0.001$).

reductions of <10% represented acceptable mechanical strength based on the previous reports [45,59]. Amongst all the AmB DMP, F3 AmB DMP were shown to be resilient to compression and could be a great candidate to deliver AmB topically.

The insertion behaviour of DMP affects the skin permeability and thus the microneedle's drug delivery performance [60]. The insertion capability is an overall outcome of various parameters including the material mechanical strength, toughness, the shape of the needles [61]. PF can act as a validated skin-simulant artificial membrane, as reported in previous studies [35]. PF test is a simple and standard test for estimating the insertion depths by multiplying the number of layers penetrated by microneedles to the thickness of each PF layer [58]. The thickness of a single PF layer is about 126 μm. Penetration into each PF layer creates holes on it and indicates an insertion depth of 126 μm. As displayed in Fig. 3B, for all the patches, more than 50% of the needles penetrated the third layer of PF (indicating an insertion depth of 378 μm) and no needles could penetrate to the fifth layer of PF (indicating an insertion depth of 630 μm). For all the patches, a decrease of over 60% was observed in all the patches from the third layer to the fourth layer of PF, indicating that the insertion depths of over 60% of the needles reached between 378 μm (the third layer) and 504 μm (the fourth layer). Even though F1 showed a higher number of holes compared to other formulations, the insertion behaviours of all the formulations are considered equivalent as most of the needles reached the same depth range based on the insertion profiles obtained using PF test [35,62]. Similar insertion profiles have been reported before for DMP capable of delivering therapeutic compounds contained in the needle tips [63–65].

3.1.4. *Ex vivo skin deposition*

Skin deposition is a crucial parameter to consider in evaluating the delivery effectiveness of DMP. The tips of DMP are generally designed in the micrometre range to elude the nerves when inserted into the skin. The tiny size limits the drug loading volume of DMP. In terms of drug loading, F1 contained the lowest drug loading per patch (1.58 ± 0.17

mg/patch) while F3, F5 and F6 contained about 3 mg per patch. Taken all the factors into consideration, formulations with high drug loading and decent insertion and mechanical properties, *i.e.* F3, F5 and F6 AmB DMP were further investigated for their ability to deliver AmB into the skin. After application and *in situ* deposition for 24 h, the drug inside the skin was extracted and analysed for all groups. As shown in Fig. 3C, all AmB DMP deposited a large amount of drug in the skin and formed yellow drug depots inside the skin. As shown in Fig. 3D, F3 and F6 AmB DMP deposited a considerate amount of drug in the skin, which reached 271.40 ± 46.14 μg/cm^2 and 222.80 ± 37.53 μg/cm^2, respectively. F5 AmB DMP deposited 97.17 ± 22.05 μg/cm^2, which was significantly different with F3 AmB DMP ($p < 0.05$). With different ratios of PVP and PVA, F3 AmB DMP, consisting of AmB, PVP, and PVA, delivered the highest amount of drug into the skin tissue. According to the literature, the hydrogen bond interaction between the carboxyl groups of PVP and hydroxyl groups of PVA should result in excellent mechanical properties for DMP [66]. Accordingly, F3 AmB DMP were chosen for further investigation.

F3 suspension used as a topical formulation was also considered in this study. As shown in Fig. 3C, little yellow drug traces were observed after the application of F3 suspension for 24 h. F3 suspension deposited 4.32 ± 1.05 μg/cm^2 in the skin, which was significantly less compared to F3 AmB DMP ($p < 0.01$) and F6 AmB DMP ($p < 0.05$). The results are in line with the literature and suggest that it is difficult for AmB to penetrate the SC, even with the addition of PVP and PVA, necessitating the use of the microneedle platform [24,25].

In another study, an ocular microneedle patch entrapping a liposome formulation was established to treat fungal keratitis. It was found to deliver about 70 μg/g within excised human cornea and about 10 μg in the donor chamber of Franz cells. This patch was effective for CA infected cornea both in an *ex vivo* model and in an *in vivo* rabbit infection model [67]. A recent study by our group designed an implantable microneedle system to deliver AmB. The microneedle system contained 160.0 ± 7.4 μg of AmB and was able to deliver 86.99% ± 11.62% of the drug from the tips into the skin [31]. Taken together, F3 AmB DMP developed in the present study were able to deliver the highest amount of 271.40 ± 46.14 μg/cm^2 AmB into the skin compared to all previously reported topical microneedle systems, indicating the promise of the system.

According to the literature, several systems for topical delivery of AmB have been developed and tested. Various nanoemulsion formulations, for instance, were proposed. One nanoemulsion using lipids and surfactants could deposit 84.7 ± 9.3 μg of AmB in a fixed diffusion area (3.104 cm^2) of abdominal rat skin, which equalled 27.3 ± 3.0 μg/cm^2 and was found to be 1.59 times higher than Fungisome®. Antifungal tests demonstrated its effect against *Aspergillus fumigatus* and CA [68]. In a different study, another nanoemulsion formulation prepared by Hussain et al. delivered 231.37 ± 3.6 μg/cm^2 in the abdominal skins of albino Wistar rats and a 2.11-fold higher enhancement ratio as compared to Fungisome® [69]. Moreover, a microemulsion formulation fabricated by Butani et al. was able to deliver 119.64 μg AmB in Albino Wistar rat skin in an application area of 1.54 cm^2, which equalled 77.69 μg/cm^2. This formulation exhibited a zone of inhibition of 5.1 mm against *Trichophyton rubrum* fungal species [70]. A solid lipid nanoparticle system was reported to deposit 40 μg of AmB in skin over an effective diffusion area of 1.54 cm^2 on female albino Wistar rat skin with an inhibition zone of 1.22 ± 0.11 mm against *Trichophyton rubrum* [71]. Additionally, for ultradeformable liposomes containing Tween 80, the total AmB accumulation in the excised human skin was 40 times higher (1.8 ± 0.1 μg/cm^2) than for AmBisome® (0.045 ± 0.002 μg/cm^2) [72]. In the present work, the *ex vivo* skin deposition of AmB in the porcine skin was studied using a Franz cell setup, followed by AmB extraction and quantification. At 24 h, the *ex vivo* porcine skin deposition of F3 AmB DMP reached 271.40 ± 46.14 μg/cm^2, which was the highest cumulative amount of AmB compared to all the relevant formulations previously described in the literature. It is also noticed that the type of biological membrane used in the skin permeation experiment significantly affects the skin permeation and deposition potential of the tested formulations. Considering the rat skin is thinner and more porous than the human skin and the neonatal porcine skin is more comparable to human skin [73], the skin deposition results obtained using *ex vivo* porcine skin are very promising.

3.2. Characterisation of AmB DMP tips

3.2.1. Particle size measurements and morphology

The particle size was measured by suspending the F3 AmB DMP tips or AmB powder in deionised water. The particle size results of reconstituted F3 AmB DMP tips and AmB powder are listed in Table 3 and the PSD of the two samples is presented in Fig. 4A. As PVP and PVA are water soluble polymers and were not chemically conjugated with AmB, the particle size detected from F3 AmB DMP tips and AmB powder was from pure AmB particles. PVA and PVA were the main components of the DMP tips and they may act as emulsifying agents and stabilisers, as previously reported [38,74]. The mean size of AmB particles in the F3 AmB DMP dry tips was distributed in the range of 0.34–13.69 μm and mean size distribution was 1.45 ± 0.01 μm, while the mean size range of AmB powder was distributed broadly in the range of 0.50–80.20 μm. With the limitation of the measuring range, the particles with a size greater than 87.50 μm were not able to be measured. Steepness factor (SF), calculated by the ratio of d_{50} to d_{20} values, was used to analyse the size distribution of F3 AmB DMP tips and AmB powder. It is reported that a curve with SF greater than 2 can be described as 'broad' and that with SF less than 2 as 'narrow' or 'steep' [75]. For F3 AmB DMP particle size curve, the SF was in the range of 1.51–1.86, which could be described as narrow distribution. While for AmB powder, the SF was in the range of 3.96–4.18, which could be described as broad distribution. The results showed that the size of the particles released from F3 AmB DMP tips was much more reduced and narrower in distribution than that of AmB powder. The size distribution of the particles released from F3 AmB DMP tips indicated that after insertion into the skin, the AmB released from the F3 AmB DMP tips were particles within the micron range and 90% of the particles were less than 5 μm. Particle size reduction is a common strategy to increase the surface area, and consequently the dissolution rate and bioavailability, of hydrophobic drugs [76]. For AmB, reports have shown that the reduction in particle size resulted in improved therapeutic effects as well as enhanced toxicity [77]. A micronised AmB formulation has been prepared using a spray drying technique with the addition of cyclodextrin polymers to improve the solubility and dissolution of AmB [78].

Micron-sized and submicron-sized particles have been loaded into the dissolving microneedles to enhance the drug permeation and drug targeting of various therapies [45,66,79–81]. Even though those results are promising, the fabrication procedures generally require milling or formulating the micron-sized or submicron-sized formulations before loading them into the tips. The tips were then cast by mixing the preformed formulation with microneedle matrices. In this study, the micron-sized drug formulations and the tip casting solution were prepared at the same time as simple as mixing drug powder with PVP and PVA polymers using a speedmixer. Advantages of this simple technique include (1) easy manufacturing procedures, (2) safe and mild preparation conditions as only aqueous solutions are used, (3) narrow particle size range, and (4) safe and commonly used pharmaceutical polymers.

The tips of F3 AmB DMP were observed on the patch using a digital

Table 3
Median diameter of percent undersize volume fraction for F3 AmB DMP tips and AmB (means ± SD, $n = 4$).

Samples	d_{10} (μm)	d_{50} (μm)	d_{90} (μm)
F3	0.78 ± 0.00	1.67 ± 0.01	4.65 ± 0.01
AmB powder	2.43 ± 0.03	21.21 ± 0.44	65.47 ± 0.70

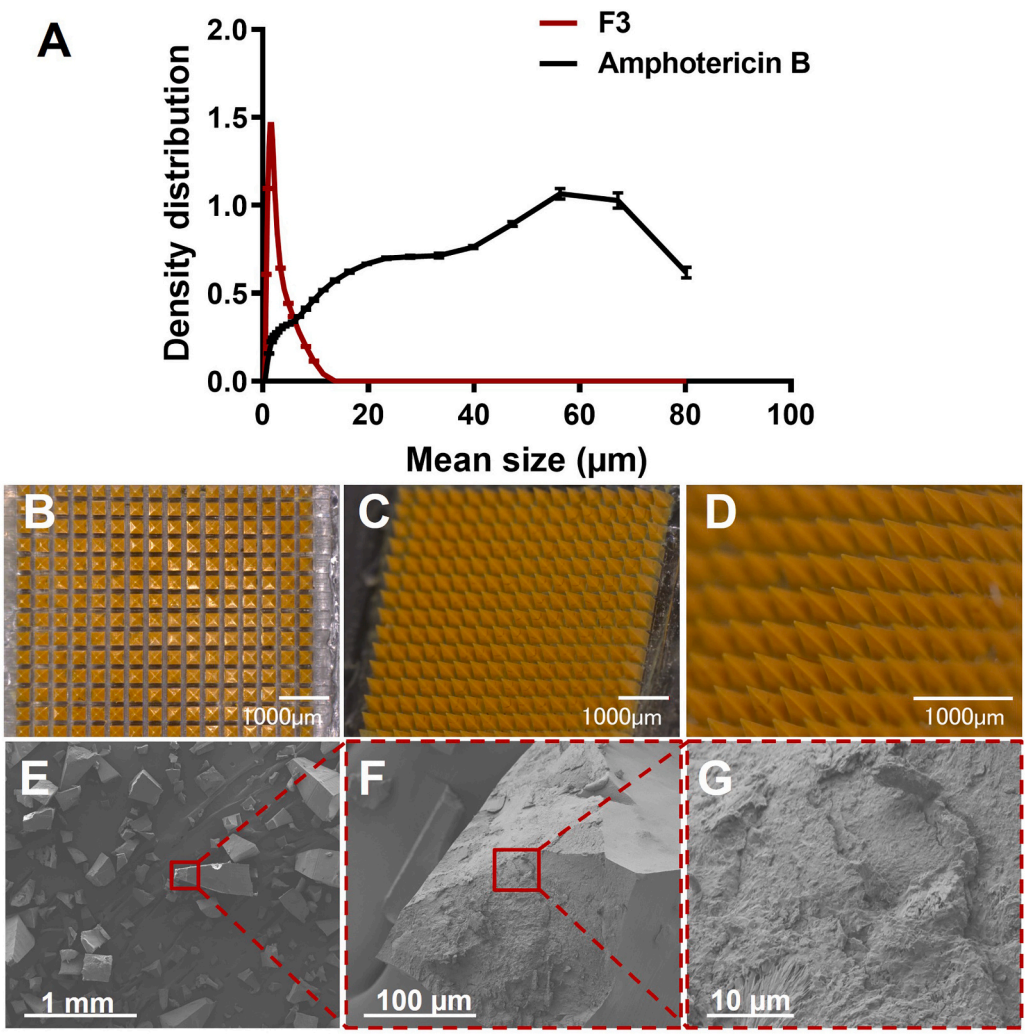

Fig. 4. Particle size measurements and morphology of F3 AmB DMP tips. (A) Mean particle size distribution of F3 AmB DMP tips and AmB powder (means ± SD, n = 4). (B) A bird's-eye view digital picture of F3 AmB DMP. Scale bar, 1000 μm. (C) A digital picture of F3 AmB DMP. Scale bar, 1000 μm. (D) A detailed digital picture of F3 AmB DMP tips. Scale bar, 1000 μm. The SEM images show the microstructure of the tips including the surface and cross-section surface morphology. (E) Scale bar, 1 mm. (F) Scale bar, 100 μm. (G) Scale bar, 10 μm.

microscope. A bird's-eye view of F3 AmB DMP (Fig. 4B) indicated that the drug was only concentrated in the tips as the base between tips showed little trace of the drug. Based on the detailed pictures (Fig. 4C and D), the tips of F3 AmB DMP appeared sharp, smooth and filled with drug. In an attempt to look into the microstructure of the tips, some F3 AmB DMP tips were broken down and the SEM was used to investigate the morphology of the tips both in the surface and the cross-section. Fig. 4E showed the surface of the AmB DMP tips was smooth. Fig. 4F and G presented that the cross-section surface of the tips was relatively smooth as well. No noticeable drug particles were easily identified by SEM. These results indicated that AmB drug particles were encapsulated within the polymeric matrix and the particles were detectable after tip dissolution in water.

3.2.2. *Thermo-gravimetric analysis*

TGA analysis was performed to evaluate if AmB formulated with PVP and PVA showed different thermal behaviour than the pure compound or the physical mixture of the F3 formulation. In particular, it aids in DSC analysis, such as analysing the water content of the formulation as well as the decomposition temperature. The TGA curves (Fig. 5A) of AmB powder and physical mixture of AmB, PVP and PVA revealed obvious thermal weight loss (5%) before 100 °C. For F3 AmB DMP tips, 2% of the weight was gradually lost before 100 °C. After 100 °C, these groups showed a similar trend with obvious thermal weight loss at 230 °C starting from 180 °C. TGA was used to analyse the thermal degradation temperature. The first step of weight loss before 100 °C could be attributed to the evaporation of adsorbed water for all the samples. The other weight loss were due to the thermal decomposition stages of the products. TGA showed that the degradation of AmB started at about 181 °C. This finding was consistent with the literature [82].

3.2.3. *Differential scanning calorimetry*

The DSC thermograms in Fig. 5B depict the thermal behaviour of AmB, physical mixture, and F3 AmB DMP tips in a range of 0–180 °C. The thermogram of AmB showed an endothermic transition around 144 °C, which was in agreement with previous reports [83,84]. This endothermic peak was also identified in the physical mixture group. DSC thermogram of F3 AmB DMP tips conducted between 0 °C and 180 °C showed a broad endothermic peak at about 160 °C. The broad shape and the peak shift from 144 °C to 160 °C indicated that the reduced crystallinity of the tips and the interaction between the drug and the polymer matrices [85,86]. The increase in temperature during DSC analysis and the relatively small particle size of micronised AmB particles in F3 AmB DMP tips may promote interaction of the AmB crystal with the polymer matrices. Reorganization of the AmB crystal may occur in the polymeric matrices' environment on heating while DSC analysis [87,88].

3.2.4. *Powder X-ray diffraction*

XRD diffraction examined the crystalline structure of the materials [89]. As noticed in Fig. 5C, AmB displayed strong sharp crystalline peaks at 13.9° and 21.5°, which has been reported previously [83,90]. No new diffractogram patterns were observed in physical mixture or F3 AmB

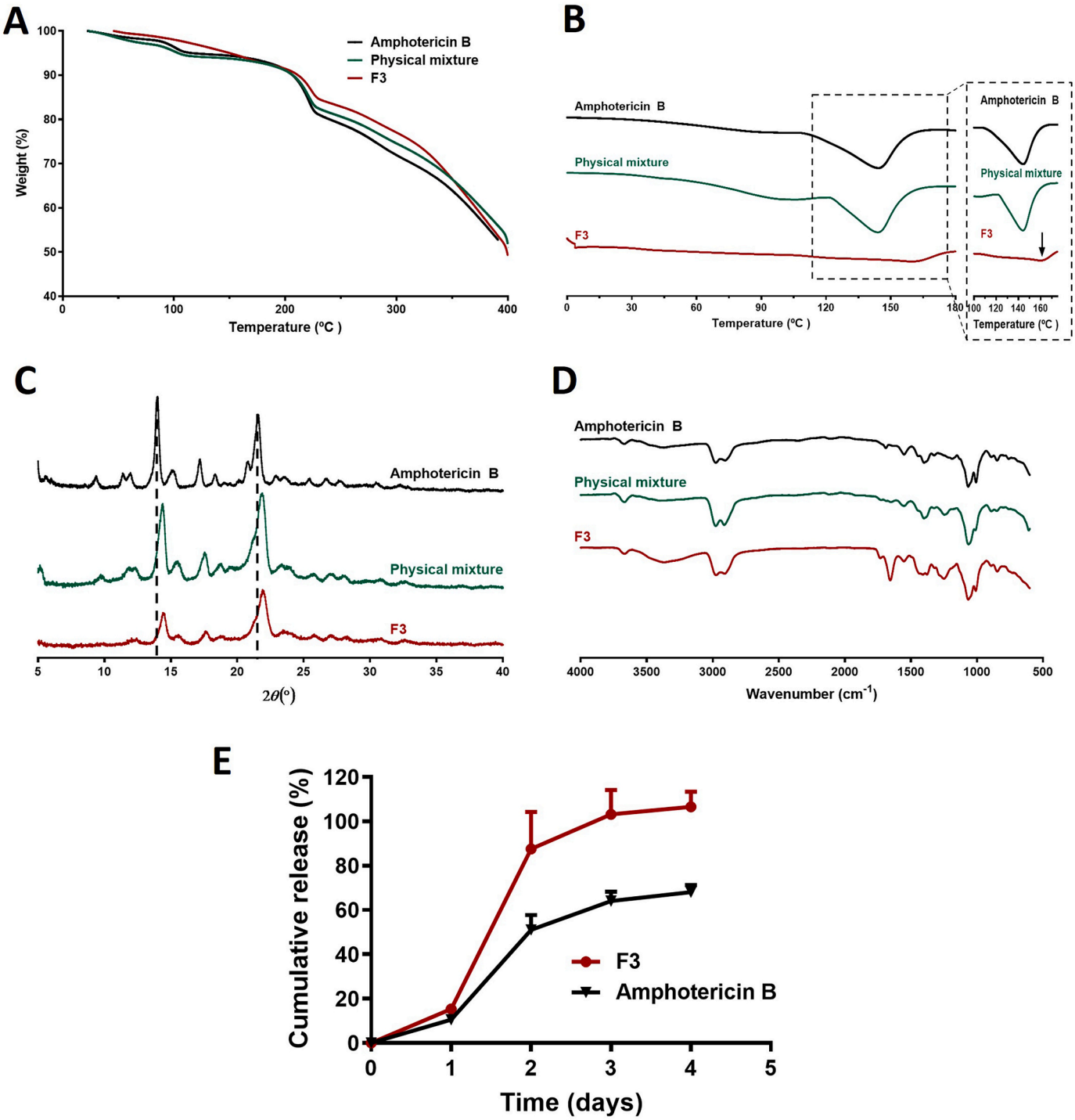

Fig. 5. Characterisation of F3 AmB DMP tips. (A) TGA thermograms, (B) DSC thermograms, (C) XRD analysis and (D) FTIR spectra of AmB powder, F3 AmB DMP tips, and physical mixture of F3 AmB DMP tip formulation. (E) *In vitro* release profile of F3 formulated tips and AmB powder. (Means ± SD, $n = 5$).

DMP tips. The physical mixture presented a similar diffractogram with AmB, which was highly crystallised and revealed intense crystalline peaks between 8° and 13°. The F3 AmB DMP tips, on the other hand, showed obviously reduced peak intensity in this region and overall broad peaks, indicating a decrease in crystallinity. These two characteristic peaks of AmB (13.9° and 21.5°) were also present in both physical mixture and F3 AmB DMP tips but the peaks were broad and slightly shift. These observations revealed the existence of AmB crystal in F3 AmB DMP tips. The broadness in shape and reduced peak intensity of the characteristic AmB peaks could be attributed to and consistent with the previous observation of the reduced particle size of AmB crystal in the F3 AmB DMP tips. These data from XRD and DSC indicated a reduced crystallinity after size reduction of the crystal, which has been extensively observed in micronised systems [91,92].

3.2.5. *Fourier transform infrared spectroscopy*

FTIR spectra from 400 cm^{-1} to 4000 cm^{-1} of AmB, physical mixture, and F3 AmB DMP tip groups are presented in Fig. 5D. The FTIR spectra of AmB powder indicated characteristic peaks at 3369.7 cm^{-1} for -OH stretching vibration, 1712.9 cm^{-1} for -CH_2, 1689 cm^{-1} for carbonyl

group stretching, and 1220.3 cm^{-1} for C=C of AmB. The FTIR spectra of the F3 AmB DMP tips exhibited no changes in AmB molecular structure. Results of FTIR analysis showed that no chemical bonds were formed during the formulation process. As DSC graphs showed some change in the F3 AmB DMP tips, there might be some non-covalent chemical interactions between the drug and the excipients used. The remarkable absorption peaks at 1656 cm^{-1} could be attributed to PVP, whose FTIR spectra are shown in the Supplementary information.

3.2.6. *In vitro release study*

The *in vitro* release profiles of AmB from F3 AmB DMP tips and bulk AmB powder are illustrated in Fig. 5E. Due to the intrinsic hydrophobicity of AmB, PBS (pH 7.4) with the addition of 1% SLS *w/v* was used as the release medium. The recovery rate of AmB in the release medium at 37 °C for 17 days was found to be over 95% (as shown in the Supplementary information). The release study showed that AmB was released faster and more completely from F3 AmB DMP tips than from the bulk drug powder. Differences in the cumulative release percentage were noticeable after 1 day, with the F3 AmB DMP tips showing a significantly higher release from this point onward ($p < 0.05$). A complete release was observed for F3 AmB DMP tips after 3–4 days, while for the bulk drug powder, only about 60% was released after 4 days.

The reduced size of the particles released from F3 AmB DMP tips compared to the bulk drug powder could explain the enhanced release of the F3 AmB DMP tips compared to the AmB powder. For hydrophobic drugs, particle size is an essential factor to be considered as it determines the biopharmaceutical and pharmacokinetic properties of the drug [93]. The size measurement results showed that the mean particle size of AmB in the F3 AmB DMP tips was much reduced compared to that in bulk AmB powder. As suggested by the modified Noyes-Whitney equation, a reduced size of the solid compound increases the surface area available for dissolution and thus improving the dissolution of hydrophobic drugs [94]. In the literature, the addition of PVP has been reported to cause a significant reduction in particle size of AmB formulations and protect the particles from aggregation [74]. PVA was also used to reduce the size of the particles of AmB formulation and to stabilize the particles as a small quantity of it could possibly absorb at the particle surface [95]. Moreover, the presence of PVP and PVA has been reported to facilitate the amorphous formation of some hydrophobic drugs [54,96,97]. PVP has also been shown to inhibit drug crystallization in solution as well as in the solid-state [96], and protect against drug degradation in solution [54]. Thermal analysis of DSC and XRD showed that the crystallinity was reduced, which also explained the enhanced release profile of the F3 AmB DMP tip group compared to the bulk drug powder.

3.3. *Antifungal performances of AmB DMP*

3.3.1. *Disk diffusion test*

Disk diffusion test results of blank DMP, F3 AmB DMP and paper discs with 3 mg of AmB, together with an untreated group against the growth of CA are displayed in Fig. 6A and B. The untreated group showed the growth of fungi cells under current culture circumstances. The blank DMP, which were made of PVP and PVA gel without AmB, had no inhibition to fungal growth, as evidenced by the fungal growth even on the site of the blank DMP application. The AmB DMP, on the other hand, showed remarkable inhibition of CA with a zone area of 389.9 ± 75.8 mm^2, which equals a circle with a radius of 11.1 ± 1.1 mm. Drug depots were observed in the agar after insertion. The paper disc with 3 mg of AmB, as much amount as loaded in the F3 AmB DMP, showed an inhibition zone of 229.7 ± 21.1 mm^2 with a radius of 8.5 ± 0.4 mm. The significant difference (****$p < 0.0001$) between F3 AmB DMP and paper discs with 3 mg AmB could be attributed to the addition of PVP and PVA promoting the diffusion of AmB to a larger area. There is no inhibition of CA growth in blank DMP, which had no significant difference ($p > 0.05$) with untreated group, indicating that PVP and PVA could not exert antifungal effects.

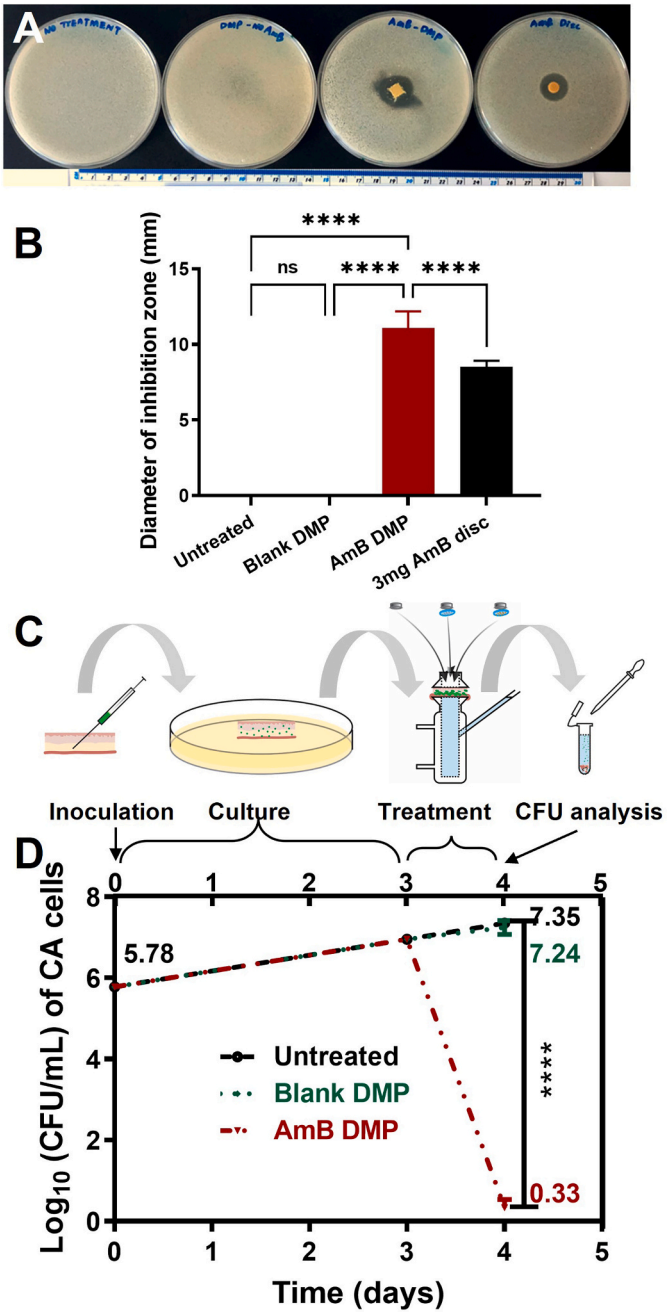

Fig. 6. Antifungal performances of AmB DMP. (A) Representative disk diffusion test results of untreated group, blank DMP, AmB DMP, and paper discs with 3 mg of AmB, respectively. (B) The diameters of the inhibition zones created by untreated group, blank DMP, AmB DMP and paper discs with 3 mg of AmB. (C) Illustration of the experimental set-up of *ex vivo* antimicrobial assay in an *ex vivo* infection model on porcine skin. Injection of CA was followed by 3 days' culture. Treatment including untreated group, blank DMP and AmB DMP on the infected skin models were performed for 1 day using Franz cell set-up. The skin samples were disrupted after treatments and CFU analysis were performed for the infected skin samples. (D) The CFU analysis results of fungi for the untreated, blank DMP treated, and AmB DMP treated agar plates, respectively. (Means ± SD, $n = 3$; ****$p < 0.0001$).

Antifungal activities of F3 AmB DMP were tested against *CA*. Candida infections are also amongst the most widespread superficial cutaneous fungal infections. CA is the major cause of wound infections, sepsis, and pneumonia in immunosuppressed patients [98]. They can invade deep tissues as well as the systemic blood circulation, which

leads to life-threatening systemic candidiasis when the immune system of a patient is weakened [72,99]. A modified disk diffusion test demonstrated the *in vitro* antifungal effect of F3 AmB DMP against *CA*. The inhibition zone of growth was not a regular circle, probably because the dissolution of AmB in the dissolving polymeric matrices and aqueous agar plates promoted the release of AmB into a larger area.

3.3.2. Antimicrobial assay in an ex vivo infection model on porcine skin

Antibiofilm activity of F3 AmB DMP was tested by applying F3 AmB DMP or blank DMP to the *ex vivo* CA infected porcine skin models. The viable fungal cells before and after the treatments were counted and compared. As shown in Fig. 6D, the viable count increased in the skin infection model from 6×10^5 CFU (day 0) to about 2.3×10^7 CFU (day 4) in the untreated group. This demonstrated the growth of the fungal cells inside the porcine skin, indicating the success of the *ex vivo* infected models. After applying blank patches for 24 h, the fungi burden on the biofilm models on day 4 showed no significant difference with the untreated group on day 4 ($p > 0.05$). This indicated that the blank DMP were not able to affect the growth of the fungi inside the skin. After applying F3 AmB DMP for 24 h, the number of fungal cells inside the porcine skin reduced from 6×10^5 CFU (day 0) to 2.7 ± 2.1 CFU (day 4). The fungal viabilities were much reduced following the 24-h administration of F3 AmB DMP, compared to the fungal burden after the blank DMP treatment ($p < 0.00001$) or the untreated group ($p < 0.00001$). The killing rate of F3 AmB DMP against CA reached 100%.

The *ex vivo* cutaneous fungal infection model mimicking the deep cutaneous fungal infection conditions model was set up by injecting CA cultures subcutaneously into porcine skin. The infected skin was cultured for 3 days for the growth of the fungi and treated for 1 day. Post-infection CFU counts in an *ex vivo* neonatal porcine skin biofilm model showed a 100% killing rate and a significant reduction in fungal burden in the F3 AmB DMP treated groups in comparison to the group treated with blank DMP or the untreated one. DMP carrying a nanocrystal form of itraconazole has been tested using a similar approach [63]. The viability of CA after applying the itraconazole nanocrystal DMP was reduced from 0.756×10^6 CFU/mL to about 0.64×10^4 CFU/mL after the application time of 24 h. After applying the itraconazole nanocrystal DMP for 48 h, the killing rate reached 100%, which was the same as F3 AmB DMP applied for 24 h. This study demonstrated the excellent fungal killing ability of F3 AmB DMP in the treatment of fungal infections in the deep cutaneous tissues.

3.4. Ex vivo delivery of AmB from AmB DMP

3.4.1. Ex vivo dermatokinetic study

An *ex vivo* dermatokinetic study was carried out using F3 AmB DMP to analyse the drug concentrations in different layers of the porcine skin and to possibly predict how long the drug would be retained in the skin [45,100]. As shown in Fig. 7A, for all the time points measured, the drug level in the dermis was the highest compared to that in the epidermis and that in the receiver compartment of the Franz cells. At 24 h, both AmB inside the epidermis and dermis reached the highest amount. For the dermis samples, the concentration of AmB deposited increased in the first hour to 154.0 ± 21.6 μg/cm^2 and remained stable at around 110 μg/cm^2. It peaked at 5 h, with a concentration of 180.4 ± 40.8 μg/cm^2. At 24 h, the drug deposited in the dermis was 179.8 ± 20.8 μg/cm^2. For the epidermis samples, an increase in the deposition of AmB was observed within the first 3 h and the concentration remained stable until 6 h. It reached the highest concentration of 56.9 ± 9.3 μg/cm^2 at 24 h. Inside the Franz cell receiver compartment, only a small amount of the drug was detected. At 24 h, the highest amount permeated was 7.06 ± 6.50 μg of the drug in the receiver compartment. These data indicated that the drug largely remained in the skin layers and the amount of drug which permeated through the skin to the receiver compartment was low after 24 h' application. This is promising for treating cutaneous fungal infections, as the drug would possibly remain localised inside the skin. One significant advantage of DMP systems over other topical or intradermal systems is that they can painlessly penetrate the SC and has the chance to deliver the drug as deep as or deeper than, as a reason of drug diffusion, the insertion depth [101,102]. The thickness of the epidermis of porcine skin is reported to range from 30 to 140 μm, and the dermal-epidermal thickness ratio ranges from 10:1 to 13: 1 in the pig [103]. As the epidermis layer is much thinner than the dermis, the drug had more volume to accumulate in the dermis though diffusion, but also sedimentation after 24 h.

According to one-compartmental analysis, the T_{max}, C_{max} and AUC_{0-24} for the dermis samples were 4.9 h, 139.4 μg/cm^2 and 3299.7 ± 31.0 h•μg/cm^2, respectively. For the epidermis samples, a one-compartmental model was not applicable, since the elimination phase was not observed in the 24-h profile. Non-compartmental analysis showed that the T_{max}, C_{max} and AUC_{0-24} for the epidermis samples was 24 h, 56.9 μg/cm^2 and 1009.8 h•μg/cm^2. For the receiver compartment samples, one-compartmental analysis was also not applicable. The non-compartmental model showed that the T_{max} for the receiver samples was 24 h, the C_{max} was 8.1 μg/cm^2 and the AUC_{0-24} of the drug in the receiver was 157.5 h•μg/cm^2. As the elimination phase was not observed in all the profiles, the MRT, $t_{1/2}$ data calculated using a one-

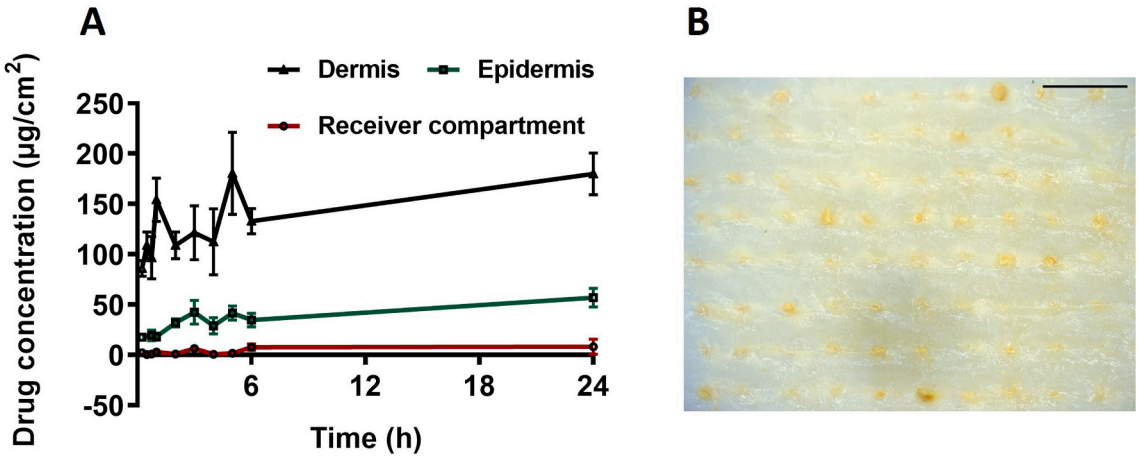

Fig. 7. *Ex vivo* dermatokinetic profiles over 24 h's application of F3 AmB DMP. (A) The concentration and time profile of AmB in the dermis, the epidermis, and the receiver compartment. ($n = 4$, means ± SD). (B) Drug depot observed on the skin after 24 h application. Scale bar 1000 μm.

compartment open model were not reliable.

The porcine skin samples after 24-h applications of AmB DMP were visualised and the representative images are presented in Fig. 7B. It was evident that the skin was penetrated by AmB DMP and that drug depots were formed inside the skin after 24 h, indicating the possibility of long-acting delivery. As described in Fig. 7A, the concentration of AmB both in the epidermis and the dermis layers remained relatively stable over several hours, increasing slightly at 24 h. This might contribute to the hydrophobic nature of AmB, which prevents the free diffusion of the drug. Another explanation for the results is that the skin lacks the enzymes to metabolise AmB. Due to the lack of elimination phase in the *ex vivo* dermatokinetic profile, an *in vitro* release study and an *in vivo* dermatokinetic study are therefore required to predict the drug release after the AmB DMP tips were inserted into the skin over 24 h.

3.4.2. *Ex vivo skin insertion performance of AmB DMP and drug distribution in the skin*

The principal purpose of this system is to deliver AmB into the deep layers of the skin, where fungal cells reside and infect the skin. To treat cutaneous fungal infections, antifungal drugs should be delivered into the deep skin tissue to kill or inhibit the growth of fungus. This is also important for other dermatological diseases such as psoriasis, inflammation, and vasculitis [104]. Accordingly, it is necessary to investigate the distribution of AmB after applying F3 AmB DMP to the skin. OCT was used to visualise the insertion of AmB DMP immediately after applying F3 AmB DMP on the skin. As observed in a representative OCT picture (Fig. 8A), F3 AmB DMP were able to penetrate the skin, exhibiting a depth of 301.34 ± 46.86 μm. As the AmB DMP tips dissolved in the skin, OCT images could not show how deep the drug could reach. Multiphoton microscopy was then applied to map the distribution of the drug inside the skin after 24 h application. Multiphoton microscopy combines laser scanning microscopy with long wavelength multiphoton excitation [105]. In this way, the near-infrared light used to stimulate multiphoton fluorescence is both scattered and absorbed less by biological tissues so that fluorescence can achieve deeper tissue penetration, efficient light detection, and reduced photobleaching [106]. As shown in Fig. 8B, a representative image from multiphoton microscopy showed the fluorescence could be detected at a distance of 170 μm beneath the skin. The three-dimensional image in Fig. 8C shows the distribution of the fluorescence inside the skin, revealing the successful delivery of AmB into the deep skin tissue. Interestingly, the drug mainly remained in the indented area caused by inserted AmB DMP tips even after 24 h. The multiphoton microscopy pictures elucidated AmB's distribution in the skin tissue after 24 h application, which is in line with the *ex vivo* dermatokinetic results in Fig. 7A. As depicted in Fig. 8C, although the drug deposited in the skin did diffuse into the nearby skin tissue after 24-h application, the fluorescence intensity in the skin indicated that the drug deposited mainly remained in the needle indented areas. Fig. 8D displays the intensity distribution of the skin observed across the depth. The intensity of the fluorescence increased from the surface of the skin, remained at a high level of 100–280 μm, and fell to zero at around 340 μm beneath the skin. In order to pierce the skin efficiently, the tips were designed sharp enough to penetrate the SC. Consequently, drugs that could be loaded in the very tips were less than in the base or middle of the individual needles. That may be the reason that the drug intensity is stronger within 100–280 μm. This data revealed that the drug deposited

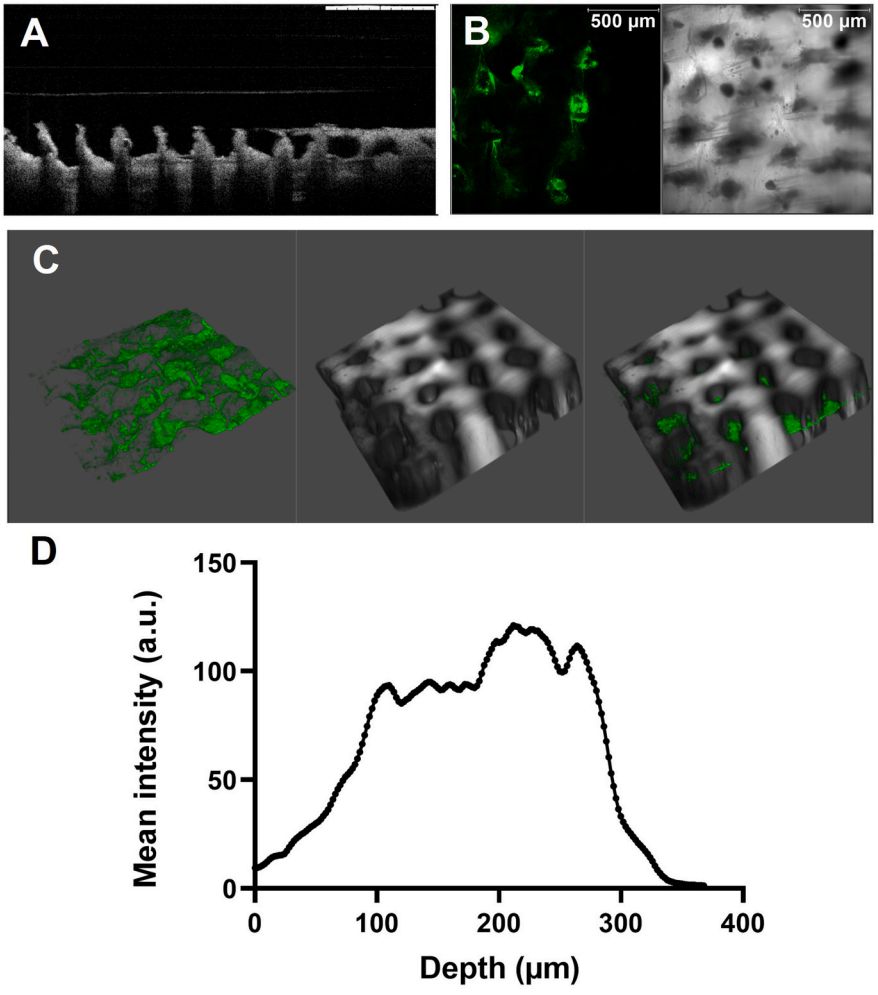

Fig. 8. Insertion depth studies. (A) Representative optical coherence tomography (OCT) picture immediately after the application of F3 AmB DMP applied to the porcine skin. Scale bar = 1 mm. (B) A representative 2D image of the x-y plane of the pierced skin at a z of 170 μm. (C) *Ex vivo* multiphoton fluorescence images of the porcine skin after applying F3 AmB DMP for 24 h. Three-dimensional image for visualising the distribution of AmB inside the skin tissue (D) The mean intensity (a.u.) across the depth of the skin after 24 h application of F3 AmB DMP.

in the skin using AmB DMP was concentrated mostly inside the skin tissue rather than on the surface. The depth of the fluorescence distribution was around 340 μm, which is similar to the AmB DMP insertion depth measured using OCT (301.34 ± 46.86 μm). In addition, the multiphoton results after 24-h application were consistent with the dermatokinetic results, indicating that the delivered AmB in the skin layer did not diffuse greatly.

3.5. *In vivo* studies

The ability of the finalised AmB DMP (F3 AmB DMP) to deliver AmB intradermally and sustain its release over an extended period of 7 days was further investigated in an *in vivo* study. *In vivo* dermatokinetics, pharmacokinetics, and biodistribution studies were performed using healthy Balb/c mice as an animal model. Fungizone®, an AmB deoxycholate formulation that has been widely used in clinical practice, was used in this experiment as a reference formulation because it was the

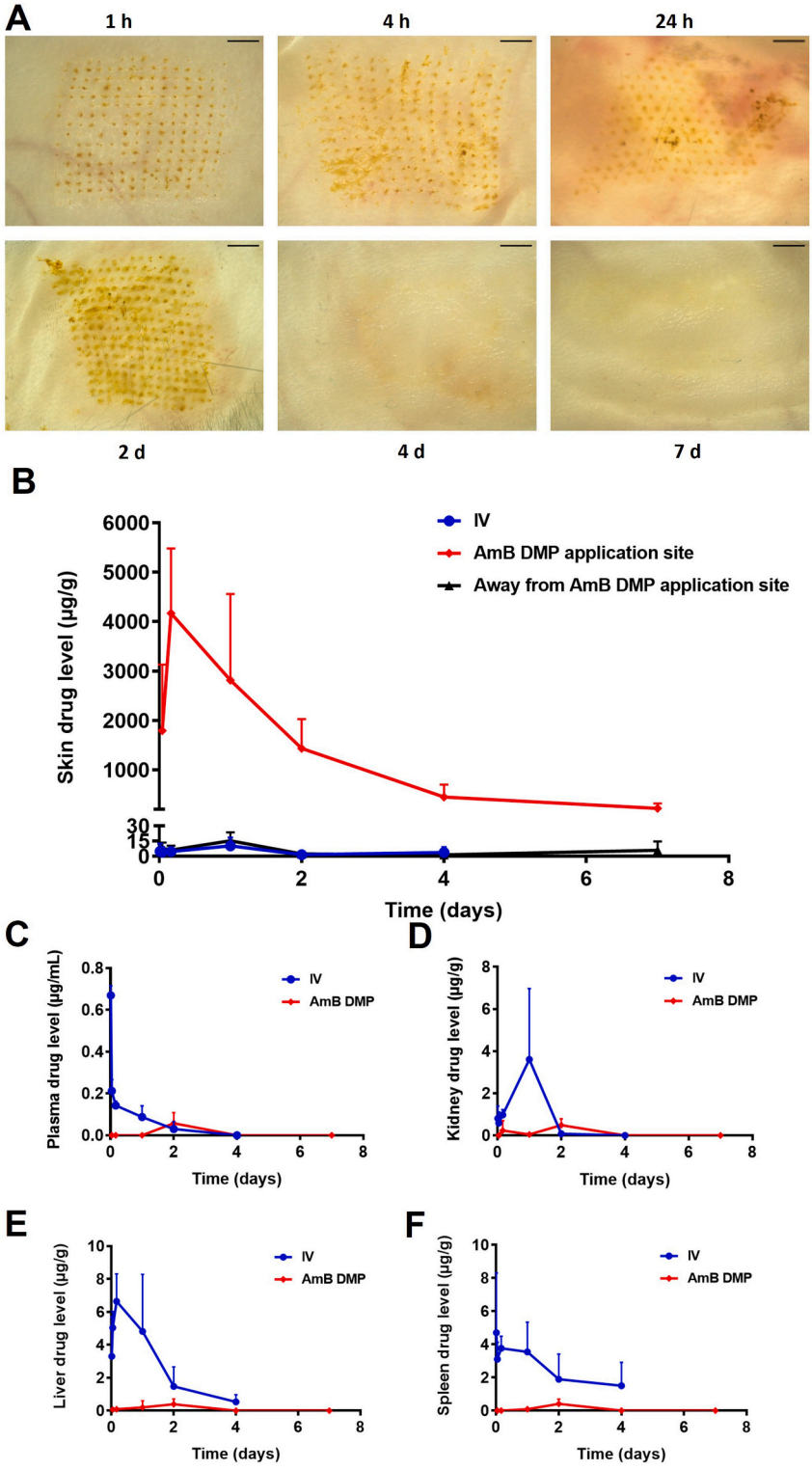

Fig. 9. *In vivo* dermatokinetic study of AmB DMP and Fungizone® intravenous bolus injection (IV). (A) The skin of mice after administration of AmB DMP at 1 h, 4 h, 24 h, 2 day, 4 day, and 7 day. (B) Dermatokinetic profiles of IV group, the application site of F3 AmB DMP and the site away from AmB DMP application site. (C) *In vivo* pharmacokinetic study result: line graph describing mean plasma concentration and time profiles of AmB after administration of AmB DMP and Fungizone® intravenous bolus injection. *In vivo* biodistribution studies results. The drug distribution profiles in (D) the kidney, (E) the liver, and (F) the spleen post-application of AmB DMP and administration of Fungizone® IV injection (Means ± SD, $n = 4$).

first AmB product approved by the US FDA with a long history of clinical use and a low cost [107]. A dose of 1 mg/kg was used as it is the highest tolerated single dose, which does not cause signs of acute toxicity, of AmB deoxycholate in BALB/c mice [108]. Accordingly, the maximum dose received of the mice with the weight of 18.86 ± 1.04 g was 18.86 ± 1.04 μg of AmB. One patch was applied in a mouse as the *ex vivo* dermatokinetic study showed the drug diffused into the Franz cell receptor compartment for one patch was 7.06 ± 6.50 μg. Two patches would probably pose a risk to exceed the maximum dose of about 20 μg per mouse. Therefore, only one patch was applied to each mouse to ensure its safety and avoid overdose.

3.5.1. *In vivo dermatokinetic study*

Since the treatment of cutaneous fungal diseases requires delivery of the antifungal drugs to the infected skin, the concentration of the antifungal drugs accumulated in the skin is a vital parameter for evaluating the delivery system. Therefore, an *in vivo* dermatokinetic study was conducted to evaluate AmB levels (reported as μg/g) in the skin after IV injection (the conventional administration route for AmB, here used as a control) and after applying F3 AmB DMP. Drug levels at the DMP application site, at 2.0 ± 0.5 cm away from the DMP application site, as well as the skin in the IV cohort were quantified using a validated HPLC method and the results are illustrated in Fig. 9B.

In cohort A, where mice received the drug by IV injection (the control group), the maximum drug level in the skin (10.16 ± 8.27 μg/g) was achieved 24 h post drug administration, after which it declined rapidly to reach 0.97 ± 0.12 μg/g on day 4. In cohort B, where mice received the drug by the finalised F3 AmB DMP, AmB concentration at the DMP application site after application of DMP for 1 h (the first sampling point) was 1792.22 ± 1336.82 μg/g. This increased rapidly to reach its maximum concentration of 4165.58 ± 1311.00 μg/g after F3 AmB DMP had been applied for 4 h. This is around 410-fold higher than the maximum concentration achieved by IV injection. After that, AmB levels in the skin decreased gradually to reach 219.07 ± 102.81 μg/g on day 7 (the last sampling point). This is still 22-fold higher than the maximum concentration achieved by IV injection. Drug level was also detected in the skin 2.0 ± 0.5 cm away from the DMP application site (Fig. 9B). Drug level in the non-application skin site was found to follow a similar trend and level as that of the IV group. The maximum AmB concentration 15.35 ± 8.20 μg/g was achieved 24 h after the DMP was applied and then declined slowly to reach its lowest level on day 7.

It is worth mentioning that drug depots (yellow) were noticed at the application site of AmB DMP after 1 h, 4 h, 1 d and 2d, as shown in Fig. 9A. After day 4 and day 7, drug depots were not easily observed. No skin irritation/erythema post-removal of AmB DMP was noticed, demonstrating the likely safety of the drug delivery system. These results demonstrated that the finalised AmB DMP was able to deliver AmB into the skin tissue in an *in vivo* setup and created depots in the skin that allowed the drug to diffuse at a very low rate to the surrounding areas for over a week.

The designed AmB DMP are intended to deliver AmB to treat cutaneous fungal infections. AmB demonstrates concentration-dependent killing against a wide range of fungi in the *in vitro* studies. Both the rate and extent of *in vitro* fungicidal effects were enhanced with the increase of AmB concentration [109]. Direct measurement of the drug at the site of action (the skin layer in this study) is likely to provide better insight into the efficacy of the products than plasma pharmacokinetics [110]. Parameters such as the maximum quantity of active drug molecules in the skin layer (C_{max}), and AUC are important in the dermatokinetics studies to extrapolate the potential therapeutic outcomes of the system. *In vivo* pharmacodynamic studies showed that therapeutic effects of AmB were associated with the drug level of AmB at the target site. A linear dose concentration-response effect was observed for *in vivo* administration of AmB [108]. In a study to deliver AmB for treating cutaneous leishmaniasis, a clear correlation between intralesional drug levels and treatment outcomes was demonstrated and was attributed to the known concentration-dependent manner in which AmB exerted its antimicrobial activity [111]. In this study, Riezk *et al* developed a novel chitosan nanoparticle system that achieved a C_{max} of about 50 μg/g of AmB in the intralesional skin site after intravenously injections of five doses in ten days. This system showed significantly higher efficacy than AmBisome® in terms of reduction of lesion size and parasite load [111]. Another study compared the dermatokinetic profiles of AmBisome® and Fungizone® single dosing or multiple IV dosing in healthy mice or leishmania infected mice. It was found the $AUC_{0.5–48}$ skin site after a single dose of 1 mg/kg Fungizone was about 1269 ± 190 h*ng/g, which was lower than the $AUC_{0\text{-}t}$ of the IV injection obtained in this study (367.40 h*μg/g) and much lower than the $AUC_{0\text{-}t}$ achieved by the finalised F3 AmB DMP on the application site (See Table 4). More importantly, the drug level in the AmB DMP application site remained high (219.07 ± 102.81 μg/g), even on day 7 post AmB DMP application.

3.5.2. *In vivo pharmacokinetic study*

Drug pharmacokinetic profiles in plasma are important for indicating the absorption of formulations into the systemic circulation. The pharmacokinetic profiles of AmB post its administration by either the finalised AmB DMP or IV injections are presented in Fig. 9C. Pharmacokinetic parameters of these *in vivo* data were calculated and are displayed in Table 5.

As shown in Fig. 9C, the drug remained undetectable in the plasma until day 2 post DMP application, where it reached 0.06 ± 0.05 μg/mL and then rapidly declined to below the LLoD on day 4. In contrast, AmB pharmacokinetic profile in plasma post IV injection has shown to be completely different. The maximum drug concentration C_{max} of 0.67 ± 0.04 μg/mL was achieved 15 min after the injection. The plasma concentration of AmB in the IV group decreased rapidly to reach 0.03 ± 0.04 μg/m on day 2 and then continued to decline to levels below LLoD on day 4. The parameters for the finalised AmB DMP group cannot be calculated due to a low level of plasma concentrations and the lack of data.

3.5.3. *In vivo biodistribution studies*

The liver, the spleen, and the kidney are the most frequent organs where AmB accumulates, and the kidney is the organ where the toxicity of AmB is most apparent [112,113]. Therefore, in this study, the drug levels in the kidney, liver, and spleen were also determined. As shown in Fig. 9D, after administration of the finalised AmB DMP, AmB was detected in the kidney at a concentration of 0.24 ± 0.48 μg/g after 4 h. Then, it fell to 0.05 ± 0.09 μg/g on day 1. After that, it reached its maximum concentration of 0.49 ± 0.30 μg/g on day 2 and then declined to a level that was lower than LLoD on day 4. In contrast, in the mice that received the drug by IV injection, AmB in the kidney was detected at 0.81 ± 0.59 μg/g after 15 min of administration. It peaked at day 1 at a concentration of 3.61 ± 3.36 μg/g and was undetectable on day 2 and day 4. The AUC of the drug level in the kidney of these two groups showed a significant difference ($p < 0.05$).

AmB levels in the liver are plotted in Fig. 9E. AmB was detectable in the liver at a concentration of 0.07 ± 0.14 μg/g at 1 h post

Table 4
Summary of *in vivo* Balb/c mice dermatokinetic parameters post-application of AmB DMP and administration of Fungizone® IV injection (means ± SD, $n = 4$).

Parameter	IV injection	AmB DMP application site	2.0 ± 0.5 cm away from AmB DMP application site
$t_{1/2}$ (h)	23.51	37.50	208.31
T_{max} (h)	24.00	4.00	24.00
C_{max} (μg/g)	10.16	4165.58	15.35
$AUC_{0\text{-}t}$(h*μg/g)	367.40	199,900.33	797.77
$AUC_{0\text{-}inf}$ (h*μg/g)	400.41	211,752.18	2549.40
MRT (h)	37.35	50.57	343.72

Table 5
Summary of *in vivo* pharmacokinetic parameters post-application of AmB DMP and administration of Fungizone® IV injection (means ± SD, n = 4).

Parameter	AmB DMP	IV injection
$t_{1/2}$ (h)	–	17.99
T_{max} (h)	48.00	0.25
C_{max} (μg/mL)	0.06	0.67
$AUC_{0\text{-}t}$ (h *μg/mL)	1.35	4.79
$AUC_{0\text{-}inf}$ (μg/g*h)	–	5.57
MRT (h)	–	23.02
Clearance (mL/h/kg)	–	179.58
V (mL/kg)	–	4662

administration of AmB DMP. Then it increased to a C_{max} of 0.40 ± 0.32 μg/g on day 2 and declined to a level undetectable on day 4 and day 7. For the IV group, a sharp increase in the concentration was noticed from 3.30 ± 2.39 μg/g at 15 min to C_{max} of 6.64 ± 1.67 μg/g at 4 h. A gradual decrease was then observed until day 4 to a concentration of 0.54 ± 0.44 μg/g. The permeation of the drug level in the liver (represented using AUC) showed a significant difference ($p < 0.001$).

Drug levels in the spleen are displayed in Fig. 9F. For the AmB DMP group, AmB was at a level lower than LLoD until day 1 at a concentration of 0.08 ± 0.17 μg/g. It peaked at 0.41 ± 0.29 μg/g on day 2 and was then undetectable on day 4 and day 7. For the IV group, the profile peaked at 15 min at a level of 4.70 ± 3.60 μg/g and decreased gradually. The drug was still detectable on day 4 at a concentration of 1.50 ± 1.40 μg/g. The AUC of AmB in the spleen was significantly higher ($p < 0.001$) in the IV group than in the AmB DMP group. In sum, AmB levels in the kidney, liver and spleen were higher in IV group than in the AmB DMP group.

The *in vivo* dermatokinetic profiles showed that when applying AmB DMP a considerable amount of the drug was deposited in the skin and the drug level in the skin reduced slowly from 5 h until day 7 after the application of F3 AmB DMP. Metabolites of AmB remain unknown thus far, and recent mass balance studies suggest that metabolism plays at most a minor role in AmB elimination [109,114]. The *in vivo* biodistribution study demonstrated the T_{max} (48 h) of the organs was in line with the T_{max} (48 h) of the plasma for the F3 AmB DMP group. These observations confirmed the efficient deposition of the drug in the skin and demonstrated that the drug deposited was distributed to the systemic circulation and the organs. The systemic deposition using F3 AmB DMP was significantly less compared to using injections in each case.

In sum, the DMP system was capable of delivering AmB locally in an efficient way and reducing systemic exposure, thus possibly reducing side effects and solving toxicity issues compared to the Fungizone®. In addition, the DMP system has the potential to allow self-administration without the intervention of healthcare professionals, which is crucially important for developing countries where fungal infections are common.

AmB is a broad-spectrum antifungal agent and has been considered as the first-line treatment of systemic fungal and parasitic infections [115]. AmB has demonstrated its effect on common medically relevant fungi, including *Candida* species, *Cryptococcus* species, *Aspergillus* species, and *mucoromycetes* [116]. Additionally, AmB has an important role in treating parasitic disease, such as leishmaniasis, which is classified as a neglected tropical disease [117]. Fungal infections and Leishmaniasis are increasingly reported in developing countries due to the environmental and host factors prevalent in such regions [118]. These countries are mainly located in tropical and sub-tropical areas providing an optimum environment for the growth of fungi and parasites. Poor hygiene and healthcare facilities are often observed [119]. In those scenarios, the AmB DMP system can be especially useful as it provides an effective and safe platform to treat cutaneous fungal infections and cutaneous leishmaniasis, as well as ease of weekly application and the potential to allow self-administration.

4. Conclusion

This study introduced an easy way to fabricate DMP loaded with AmB microparticles and suggested that the use of DMP offers great potential for the successful localised and sustained intradermal delivery of AmB. The fabricated AmB DMP were mechanically strong and can hold about 3 mg of AmB. The particle size loaded AmB was found to be within micron size range and of narrow size distribution. *Ex vivo* skin insertion and dermatokinetic studies revealed that AmB DMP deposited the drug mainly in the dermis. Finally, *in vivo* studies revealed that AmB DMP yielded very limited exposure in the plasma, kidney, liver, and spleen, compared to Fungizone® injection. It is important to highlight that one patch application can form drug depots in the skin, maintain a high drug level in the application site and sustain the release of the drug in mice over the period of a week. Overall, this paper introduces a novel and easy to fabricate DMP system to deliver hydrophobic drugs intradermally with prolonged and localised release profiles as well as less systemic exposure, which can be widely used for effective and toxic hydrophobic therapies. Leading on from these encouraging results, forthcoming studies should include *in vivo* safety and efficacy studies.

Acknowledgements

This work was supported by China Scholarship Council. We would like to thank Mr. Justin O'Hagan from English Language Support, Faculty of Medicine, Health and Life Sciences in Queen's University Belfast for language editing and proofreading this paper. We would also like to thank Dr. Akmal Sabri for his assistance with designing the illustration in this manuscript and Mr. Kaijie Qian as well as Mr. Achmad Himawan for their help with DSC and XRD analysis.

Appendix A. Supplementary data

Supplementary data to this article can be found online at https://doi.org/10.1016/j.jconrel.2021.10.001.

References

[1] F. Bongomin, S. Gago, R.O. Oladele, D.W. Denning, Global and multi-national prevalence of fungal diseases—estimate precision, J. Fungi. 3 (2017) 57, https://doi.org/10.3390/jof3040057.
[2] P. Zhou, Z. Liu, Y. Chen, Y. Xiao, X. Huang, X.G. Fan, Bacterial and fungal infections in COVID-19 patients: a matter of concern, Infect. Control Hosp. Epidemiol. 41 (2020) 1124–1125, https://doi.org/10.1017/ice.2020.156.
[3] G. Song, G. Liang, W. Liu, Fungal co-infections associated with global COVID-19 pandemic: a clinical and diagnostic perspective from China, Mycopathologia. 185 (2020) 599–606, https://doi.org/10.1007/s11046-020-00462-9.
[4] S. Sharma, M. Grover, S. Bhargava, S. Samdani, T. Kataria, Post coronavirus disease mucormycosis: a deadly addition to the pandemic spectrum, J. Laryngol. Otol. (2021) 1–6, https://doi.org/10.1017/S0022215121000992.
[5] N. Akhtar, A. Verma, K. Pathak, Topical delivery of drugs for the effective treatment of fungal infections of skin, Curr. Pharm. Des. 21 (2015) 2892–2913, https://doi.org/10.2174/1381612821666150428150456.
[6] A.A. Kyle, M.V. Dahl, Topical therapy for fungal infections, Am. J. Clin. Dermatol. 5 (2004) 443–451, https://doi.org/10.2165/00128071-200405060-00009.
[7] V.M. Espinosa-Hernández, V. Morales-Pineda, E. Martínez-Herrera, Skin infections caused by emerging Candida species, Curr. Fungal Infect. Rep. 14 (2020) 99–105, https://doi.org/10.1007/s12281-020-00380-9.
[8] H. Degreef, J. Heeres, M. Borgers, Antifungal azoles for skin disorders, Expert Opin. Ther. Pat. 16 (2006) 1235–1253, https://doi.org/10.1517/13543776.16.9.1235.
[9] S. Benedict, J. Colagreco, Fungal infections associated with malignancies, treatments, and AIDS, Cancer Nurs. 17 (1994) 411–417.
[10] P. Zan, A. Than, P.K. Duong, J. Song, C. Xu, P. Chen, Antimicrobial microneedle patch for treating deep cutaneous fungal infection, Adv. Ther. 2 (2019) 1900064, https://doi.org/10.1002/adtp.201900064.
[11] A.J. Charles, Superficial cutaneous fungal infections in tropical countries, Dermatol. Ther. 22 (2009) 550–559, https://doi.org/10.1111/j.1529-8019.2009.01276.x.
[12] F.B. Cavassin, J.L. Baú-Carneiro, R.R. Vilas-Boas, F. Queiroz-Telles, Sixty years of amphotericin B: an overview of the main antifungal agent used to treat invasive fungal infections, Infect. Dis. Ther. 10 (2021) 115–147, https://doi.org/10.1007/s40121-020-00382-7.

[13] R. Fernández-García, E. de Pablo, M.P. Ballesteros, D.R. Serrano, Unmet clinical needs in the treatment of systemic fungal infections: the role of amphotericin B and drug targeting, Int. J. Pharm. 525 (2017) 139–148, https://doi.org/10.1016/j.ijpharm.2017.04.013.

[14] D. Garg, V. Muthu, I.S. Sehgal, R. Ramachandran, H. Kaur, A. Bhalla, G.D. Puri, A. Chakrabarti, R. Agarwal, Coronavirus disease (Covid-19) associated mucormycosis (CAM): case report and systematic review of literature, Mycopathologia. 186 (2021) 289–298, https://doi.org/10.1007/s11046-021-00528-2.

[15] R. Saral, Candida and Aspergillus infections in immunocompromised patients: an overview, Rev. Infect. Dis. 13 (1991) 487–492, https://doi.org/10.1093/clinids/13.3.487.

[16] F.B. Cavassin, J.L. Baú-Carneiro, R.R. Vilas-Boas, F. Queiroz-Telles, Sixty years of amphotericin B: an overview of the Main antifungal agent used to treat invasive fungal infections, Infect. Dis. Ther. 10 (2021) 115–147, https://doi.org/10.1007/s40121-020-00382-7.

[17] F. Gigliotti, J.L. Shenep, L. Lott, D. Thornton, Induction of prostaglandin synthesis as the mechanism responsible for the chills and fever produced by infusing amphotericin B, J. Infect. Dis. 156 (1987) 784–789, https://doi.org/10.1093/infdis/156.5.784.

[18] I.A. Tekko, A.D. Permana, L. Vora, T. Hatahet, H.O. McCarthy, R.F. Donnelly, Localised and sustained intradermal delivery of methotrexate using nanocrystal-loaded microneedle arrays: potential for enhanced treatment of psoriasis, Eur. J. Pharm. Sci. 152 (2020) 105469, https://doi.org/10.1016/j.ejps.2020.105469.

[19] L.K. Vora, K. Moffatt, I.A. Tekko, A.J. Paredes, F. Volpe-Zanutto, D. Mishra, K. Peng, R. Raj Singh Thakur, R.F. Donnelly, Microneedle array systems for long-acting drug delivery, Eur. J. Pharm. Biopharm. 159 (2021) 44–76, https://doi.org/10.1016/j.ejpb.2020.12.006.

[20] L. Han, J. Xue, L. Wang, K. Peng, Z. Zhang, T. Gong, X. Sun, An injectable, low-toxicity phospholipid-based phase separation gel that induces strong and persistent immune responses in mice, Biomaterials. 105 (2016) 185–194, https://doi.org/10.1016/j.biomaterials.2016.08.007.

[21] K. Peng, C. Wu, G. Wei, J. Jiang, Z. Zhang, X. Sun, Implantable sandwich PHBHHx film for burst-free controlled delivery of thymopentin peptide, Acta Pharm. Sin. B 8 (2018) 432–439, https://doi.org/10.1016/j.apsb.2018.03.003.

[22] A.S. Rzhevskiy, T.R.R. Singh, R.F. Donnelly, Y.G. Anissimov, Microneedles as the technique of drug delivery enhancement in diverse organs and tissues, J. Control. Release 270 (2018) 184–202, https://doi.org/10.1016/j.jconrel.2017.11.048.

[23] M.R. Jaafari, M. Hatamipour, S.H. Alavizadeh, A. Abbasi, Z. Saberi, S. Rafati, Y. Taslimi, A.M. Mohammadi, A. Khamesipour, Development of a topical liposomal formulation of amphotericin B for the treatment of cutaneous leishmaniasis, Int. J. Parasitol. Drugs Drug Resist. 11 (2019) 156–165, https://doi.org/10.1016/j.ijpddr.2019.09.004.

[24] F. Zhou, H. Xu, Z. Song, L. Zhu, S. Feng, R. Feng, α-Linolenic acid-modified pluronic 127-CS copolymeric micelles for the skin targeted delivery of amphotericin B, New J. Chem. 43 (2019) 444–453, https://doi.org/10.1039/c8nj03847c.

[25] L. López, I. Vélez, C. Asela, C. Cruz, F. Alves, S. Robledo, B. Arana, A phase II study to evaluate the safety and efficacy of topical 3% amphotericin B cream (Anfoleish) for the treatment of uncomplicated cutaneous leishmaniasis in Colombia, PLoS Negl. Trop. Dis. 12 (2018), https://doi.org/10.1371/journal.pntd.0006653.

[26] D. Ramadon, A.D. Permana, A.J. Courtenay, M.T.C. McCrudden, I.A. Tekko, E. McAlister, Q.K. Anjani, E. Utomo, H.O. McCarthy, R.F. Donnelly, Development, evaluation, and pharmacokinetic assessment of polymeric microarray patches for transdermal delivery of vancomycin hydrochloride, Mol. Pharm. 17 (2020) 3353–3368, https://doi.org/10.1021/acs.molpharmaceut.0c00431.

[27] L.K. Vora, A.J. Courtenay, I.A. Tekko, E. Larrañeta, R.F. Donnelly, Pullulan-based dissolving microneedle arrays for enhanced transdermal delivery of small and large biomolecules, Int. J. Biol. Macromol. 146 (2020) 290–298, https://doi.org/10.1016/j.ijbiomac.2019.12.184.

[28] Á. Cárcamo-Martínez, B. Mallon, J. Domínguez-Robles, L.K. Vora, Q.K. Anjani, R. F. Donnelly, Hollow microneedles: a perspective in biomedical applications, Int. J. Pharm. 599 (2021) 120455, https://doi.org/10.1016/j.ijpharm.2021.120455.

[29] E. McAlister, M. Kirkby, J. Domínguez-Robles, A.J. Paredes, Q.K. Anjani, K. Moffatt, L.K. Vora, A.R.J. Hutton, P.E. McKenna, E. Larrañeta, R.F. Donnelly, The role of microneedle arrays in drug delivery and patient monitoring to prevent diabetes induced fibrosis, Adv. Drug Deliv. Rev. 175 (2021) 113825, https://doi.org/10.1016/j.addr.2021.06.002.

[30] L. Han, K. Peng, L.-Y. Qiu, M. Li, J.-H. Ruan, L.-L. He, Z.-X. Yuan, Hitchhiking on controlled-release drug delivery systems: opportunities and challenges for cancer vaccines, Front. Pharmacol. 12 (2021) 1149, https://doi.org/10.3389/fphar.2021.679602.

[31] K. Peng, L.K. Vora, J. Domínguez-Robles, Y.A. Naser, M. Li, E. Larrañeta, R. F. Donnelly, Hydrogel-forming microneedles for rapid and efficient skin deposition of controlled release tip-implants, Mater. Sci. Eng. C 127 (2021) 112226, https://doi.org/10.1016/j.msec.2021.112226.

[32] R.F. Donnelly, E. Larrañeta, Microarray patches: potentially useful delivery systems for long-acting nanosuspensions, Drug Discov. Today 23 (2018) 1026–1033, https://doi.org/10.1016/j.drudis.2017.10.013.

[33] P. González-Vázquez, E. Larrañeta, M.T.C. McCrudden, C. Jarrahian, A. Rein-Weston, M. Quintanar-Solares, D. Zehrung, H. McCarthy, A.J. Courtenay, R. F. Donnelly, Transdermal delivery of gentamicin using dissolving microneedle arrays for potential treatment of neonatal sepsis, J. Control. Release 265 (2017) 30–40, https://doi.org/10.1016/j.jconrel.2017.07.032.

[34] R.F. Donnelly, R. Majithiya, T. Raghu, R. Singh, D.I.J.J. Morrow, M.J. Garland, Y. K. Demir, K. Migalska, E. Ryan, D. Gillen, C.J. Scott, A.D. Woolfson, T.R.R. Singh, D.I.J.J. Morrow, M.J. Garland, Y.K. Demir, K. Migalska, E. Ryan, D. Gillen, C. J. Scott, A.D. Woolfson, Design, optimization and characterisation of polymeric microneedle arrays prepared by a novel laser-based micromoulding technique, Pharm. Res. 28 (2011) 41–57, https://doi.org/10.1007/s11095-010-0169-8.

[35] E. Larrañeta, J. Moore, E.M. Vicente-Pérez, P. González-Vázquez, R. Lutton, A. D. Woolfson, R.F. Donnelly, A proposed model membrane and test method for microneedle insertion studies, Int. J. Pharm. 472 (2014) 65–73, https://doi.org/10.1016/j.ijpharm.2014.05.042.

[36] A. Ripolin, J. Quinn, E. Larrañeta, E.M. Vicente-Perez, J. Barry, R.F. Donnelly, Successful application of large microneedle patches by human volunteers, Int. J. Pharm. 521 (2017) 92–101, https://doi.org/10.1016/j.ijpharm.2017.02.011.

[37] A. Summerfield, F. Meurens, M.E. Ricklin, The immunology of the porcine skin and its value as a model for human skin, Mol. Immunol. 66 (2015) 14–21, https://doi.org/10.1016/j.molimm.2014.10.023.

[38] L.K. Vora, P.R. Vavia, E. Larrañeta, S.E.J. Bell, R.F. Donnelly, Novel nanosuspension-based dissolving microneedle arrays for transdermal delivery of a hydrophobic drug, J. Interdiscip. Nanomed. 3 (2018) 89–101, https://doi.org/10.1002/jin2.41.

[39] J. Domínguez-Robles, C. Mancinelli, E. Mancuso, I. García-Romero, B.F. Gilmore, L. Casettari, E. Larrañeta, D.A. Lamprou, 3D printing of drug-loaded thermoplastic polyurethane meshes: a potential material for soft tissue reinforcement in vaginal surgery, Pharmaceutics. 12 (2020) 63, https://doi.org/10.3390/pharmaceutics12010063.

[40] R.D. Boehm, P.R. Miller, W.A. Schell, J.R. Perfect, R.J. Narayan, Inkjet printing of amphotericin B onto biodegradable microneedles using piezoelectric inkjet printing, JOM. 65 (2013) 525–533, https://doi.org/10.1007/s11837-013-0574-7.

[41] N.K. Martin, J. Domínguez-Robles, S.A. Stewart, V.A. Cornelius, Q.K. Anjani, E. Utomo, I. García-Romero, R.F. Donnelly, A. Margariti, D.A. Lamprou, E. Larrañeta, Fused deposition modelling for the development of drug loaded cardiovascular prosthesis, Int. J. Pharm. 595 (2021) 120243, https://doi.org/10.1016/j.ijpharm.2021.120243.

[42] E. Mathew, J. Domínguez-Robles, S.A. Stewart, E. Mancuso, K. O'Donnell, E. Larrañeta, D.A. Lamprou, Fused deposition modeling as an effective tool for anti-infective dialysis catheter fabrication, ACS Biomater. Sci. Eng. 5 (2019) 6300–6310, https://doi.org/10.1021/acsbiomaterials.9b01185.

[43] N. Alhusein, I.S. Blagbrough, M.L. Beeton, A. Bolhuis, P.A. De Bank, Electrospun zein/PCL fibrous matrices release tetracycline in a controlled manner, killing Staphylococcus aureus both in biofilms and ex vivo on pig skin, and are compatible with human skin cells, Pharm. Res. 33 (2016) 237–246, https://doi.org/10.1007/s11095-015-1782-3.

[44] V. Kassis, J. Søndergaard, Heat-separation of normal human skin for epidermal and dermal prostaglandin analysis, Arch. Dermatol. Res. 273 (1982) 301–306, https://doi.org/10.1007/BF00409259.

[45] A.D. Permana, I.A. Tekko, M.T.C. McCrudden, Q.K. Anjani, D. Ramadon, H. O. McCarthy, R.F. Donnelly, Solid lipid nanoparticle-based dissolving microneedles: a promising intradermal lymph targeting drug delivery system with potential for enhanced treatment of lymphatic filariasis, J. Control. Release 316 (2019) 34–52, https://doi.org/10.1016/j.jconrel.2019.10.004.

[46] Y. Zhang, M. Huo, J. Zhou, S. Xie, PKSolver: an add-in program for pharmacokinetic and pharmacodynamic data analysis in Microsoft excel, Comput. Methods Prog. Biomed. 99 (2010) 306–314, https://doi.org/10.1016/j.cmpb.2010.01.007.

[47] International conference on harmonisation of technical requirements for registration of pharmaceuticals for human use, in: ICH Harmonised Tripartite Guideline - Validation of Analytical Procedures: Text and Methodology Q2 (R1), 2005.

[48] EMA, Committee for Medicinal Products for Human Use. Guideline on Bioanalytical Method Validation. www.ema.europa.eu/contact, 2012 (accessed June 3, 2021).

[49] L.B. Jenkins, F.E. Kredel, W.M. McCord, Evaluation of polyvinyl pyrrolidone as a plasma expander, Arch. Surg. 72 (1956) 612, https://doi.org/10.1001/archsurg.1956.01270220060007.

[50] M.I. Baker, S.P. Walsh, Z. Schwartz, B.D. Boyan, A review of polyvinyl alcohol and its uses in cartilage and orthopedic applications, J. Biomed. Mater. Res. Part B Appl. Biomater. 100B (2012) 1451–1457, https://doi.org/10.1002/jbm.b.32694.

[51] A.A. Albadr, L.K. Vora, A.A. Ali, G. Laverty, R.F. Donnelly Queen's University, B. Raghu, R. Thakur, Rapidly Dissolving Microneedle Patch of Amphotericin-B for Intracorneal Fungal Infections, (n.d.). doi:10.21203/rs.3.rs-486620/v1.

[52] S. Abdelghany, I.A. Tekko, L. Vora, E. Larrañeta, A.D. Permana, R.F. Donnelly, Nanosuspension-based dissolving microneedle arrays for intradermal delivery of curcumin, Pharmaceutics. 11 (2019), https://doi.org/10.3390/pharmaceutics11070308.

[53] I. Tekko, L. Vora, M.T.C. McCrudden, C. Jarrahian, A. Rein-Weston, D. Zehrung, P. Giffen, H.O. McCarthy, R.F. Donnelly, Novel Dissolving Bilayer Microarray Patches as a Minimally Invasive, Efficient Intradermal Delivery System for a Long-Acting Cabotegravir Nanosuspension, in: 2019 Control, Release Soc. Annu. Meet. Expo, Valencia, 2019.

[54] E. Charvalos, M.N. Tzatzarakis, F. Van Bambeke, P.M. Tulkens, A.M. Tsatsakis, G. N. Tzanakakis, M.P. Mingeot-Leclercq, Water-soluble amphotericin B-polyvinylpyrrolidone complexes with maintained antifungal activity against Candida spp. and *Aspergillus* spp. and reduced haemolytic and cytotoxic effects, J. Antimicrob. Chemother. 57 (2006) 236–244, https://doi.org/10.1093/jac/dki455.

[55] M.R. Zare, M. Khorram, S. Barzegar, B. Sarkari, Q. Asgari, S. Ahadian, K. Zomorodian, Dissolvable carboxymethyl cellulose/polyvinylpyrrolidone microneedle arrays for transdermal delivery of amphotericin B to treat cutaneous leishmaniasis, Int. J. Biol. Macromol. 182 (2021) 1310–1321, https://doi.org/10.1016/j.ijbiomac.2021.05.075.
[56] R. Sachan, P. Jaipan, J.Y. Zhang, S. Degan, D. Erdmann, J. Tedesco, L. Vanderwal, S.J. Stafslien, I. Negut, A. Visan, G. Dorcioman, G. Socol, R. Cristescu, D. B. Chrisey, R.J. Narayan, Printing amphotericin B on microneedles using matrixassisted pulsed laser evaporation, Int. J. Bioprinting. 3 (2017) 147–157, https://doi.org/10.18063/IJB.2017.02.004.
[57] A.S. Cordeiro, I.A. Tekko, M.H. Jomaa, L. Vora, E. McAlister, F. Volpe-Zanutto, M. Nethery, P.T. Baine, N. Mitchell, D.W. McNeill, R.F. Donnelly, Two-photon polymerisation 3D printing of microneedle array templates with versatile designs: Application in the development of polymeric drug delivery systems, Pharm. Res. 37 (2020), https://doi.org/10.1007/s11095-020-02887-9.
[58] A.H. Sabri, Y. Kim, M. Marlow, D.J. Scurr, J. Segal, A.K. Banga, L. Kagan, J.B. Lee, Intradermal and transdermal drug delivery using microneedles – fabrication, performance evaluation and application to lymphatic delivery, Adv. Drug Deliv. Rev. 153 (2020) 195–215, https://doi.org/10.1016/j.addr.2019.10.004.
[59] B. Pamornpathomkul, T. Ngawhirunpat, I.A. Tekko, L. Vora, H.O. McCarthy, R. F. Donnelly, Dissolving polymeric microneedle arrays for enhanced site-specific acyclovir delivery, Eur. J. Pharm. Sci. 121 (2018) 200–209, https://doi.org/10.1016/j.ejps.2018.05.009.
[60] B. Al-Qallaf, D.B. Das, D. Mori, Z. Cui, Modelling transdermal delivery of high molecular weight drugs from microneedle systems, Philos. Trans. R. Soc. A Math. Phys. Eng. Sci. 365 (2007) 2951–2967, https://doi.org/10.1098/rsta.2007.0003.
[61] P. Makvandi, M. Kirkby, A.R.J. Hutton, M. Shabani, C.K.Y. Yiu, Z. Baghbantaraghdari, R. Jamaledin, M. Carlotti, B. Mazzolai, V. Mattoli, R. F. Donnelly, Engineering microneedle patches for improved penetration: analysis, skin models and factors affecting needle insertion, Nano-Micro Lett. 13 (2021) 93, https://doi.org/10.1007/s40820-021-00611-9.
[62] A.R.J. Hutton, H.L. Quinn, P.J. McCague, C. Jarrahian, A. Rein-Weston, P. S. Coffey, E. Gerth-Guyette, D. Zehrung, E. Larrañeta, R.F. Donnelly, Transdermal delivery of vitamin K using dissolving microneedles for the prevention of vitamin K deficiency bleeding, Int. J. Pharm. 541 (2018) 56–63, https://doi.org/10.1016/j.ijpharm.2018.02.031.
[63] A.D. Permana, A.J. Paredes, F. Volpe-Zanutto, Q.K. Anjani, E. Utomo, R. F. Donnelly, Dissolving microneedle-mediated dermal delivery of itraconazole nanocrystals for improved treatment of cutaneous candidiasis, Eur. J. Pharm. Biopharm. 154 (2020) 50–61, https://doi.org/10.1016/j.ejpb.2020.06.025.
[64] A.J. Paredes, F. Volpe-Zanutto, A.D. Permana, A.J. Murphy, C.J. Picco, L.K. Vora, J.A. Coulter, R.F. Donnelly, Novel tip-loaded dissolving and implantable microneedle array patches for sustained release of finasteride, Int. J. Pharm. 606 (2021) 120885, https://doi.org/10.1016/j.ijpharm.2021.120885.
[65] S. Rojekar, L.K. Vora, I.A. Tekko, F. Volpe-Zanutto, H.O. McCarthy, P.R. Vavia, R. F. Ryan, Etravirine-loaded dissolving microneedle arrays for long-acting delivery, Eur. J. Pharm. Biopharm. 165 (2021) 41–51, https://doi.org/10.1016/j.ejpb.2021.04.024.
[66] A. Dian Permana, M. Mir, E. Utomo, R.F. Donnelly, Bacterially sensitive nanoparticle-based dissolving microneedles of doxycycline for enhanced treatment of bacterial biofilm skin infection: a proof of concept study, Int. J. Pharm. (2020) 119–220, https://doi.org/10.1016/j.ijpharm.2020.119220.
[67] G. Roy, R.D. Galigama, V.S. Thorat, L.S. Mallela, S. Roy, P. Garg, V.V. K. Venuganti, Amphotericin B containing microneedle ocular patch for effective treatment of fungal keratitis, Int. J. Pharm. 572 (2019) 118808, https://doi.org/10.1016/j.ijpharm.2019.118808.
[68] A. Hussain, S. Singh, T.J. Webster, F.J. Ahmad, New perspectives in the topical delivery of optimized amphotericin B loaded nanoemulsions using excipients with innate anti-fungal activities: a mechanistic and histopathological investigation, Nanomedicine 13 (2017) 1117–1126, https://doi.org/10.1016/j.nano.2016.12.002.
[69] A. Hussain, A. Samad, I. Nazish, F.J. Ahmed, Nanocarrier-based topical drug delivery for an antifungal drug, Drug Dev. Ind. Pharm. 40 (2014) 527–541, https://doi.org/10.3109/03639045.2013.771647.
[70] D. Butani, C. Yewale, A. Misra, Amphotericin B topical microemulsion: formulation, characterization and evaluation, Colloids Surf. B: Biointerfaces 116 (2014) 351–358, https://doi.org/10.1016/j.colsurfb.2014.01.014.
[71] D. Butani, C. Yewale, A. Misra, Topical amphotericin B solid lipid nanoparticles: design and development, Colloids Surf. B: Biointerfaces 139 (2016) 17–24, https://doi.org/10.1016/j.colsurfb.2015.07.032.
[72] A.P. Perez, M.J. Altube, P. Schilrreff, G. Apezteguia, F.S. Celes, S. Zacchino, C. I. de Oliveira, E.L. Romero, M.J. Morilla, Topical amphotericin B in ultradeformable liposomes: formulation, skin penetration study, antifungal and antileishmanial activity in vitro, Colloids Surf. B: Biointerfaces 139 (2016) 190–198, https://doi.org/10.1016/j.colsurfb.2015.12.003.
[73] L. Kaur, K. Singh, S. Paul, S. Singh, S. Singh, S.K. Jain, A mechanistic study to determine the structural similarities between artificial membrane Strat-MTM and biological membranes and its application to carry out skin permeation study of amphotericin B Nanoformulations, AAPS PharmSciTech 19 (2018) 1606–1624, https://doi.org/10.1208/s12249-018-0959-6.
[74] B.T. AL-Quadeib, M.A. Radwan, L. Siller, B. Horrocks, M.C. Wright, Stealth amphotericin B nanoparticles for oral drug delivery: in vitro optimization, Saudi Pharm. J. 23 (2015) 290–302, https://doi.org/10.1016/j.jsps.2014.11.004.
[75] M. Uçurum, Ö. Güleç, M. Cingitaş, Wet grindability of calcite to ultra-fine sizes in conventional ball mill, Part. Sci. Technol. 33 (2015) 342–348, https://doi.org/10.1080/02726351.2014.970313.
[76] R. Al-Kassas, M. Bansal, J. Shaw, Nanosizing techniques for improving bioavailability of drugs, J. Control. Release 260 (2017) 202–212, https://doi.org/10.1016/j.jconrel.2017.06.003.
[77] J.E. Bennett, G.J. Hill, W.T. Butler, C.W. Emmons, Correlation of particle size of intravenous amphotericin B with toxic and chemoterapeutic effects, Antimicrob. Agents Chemother. 161 (1963) 745–752.
[78] L. Mehenni, M. Lahiani-Skiba, G. Ladam, F. Hallouard, M. Skiba, Preparation and characterization of spherical amorphous solid dispersion with amphotericin B, Pharmaceutics. 10 (2018) 235, https://doi.org/10.3390/pharmaceutics10040235.
[79] M.T.C. Mc Crudden, E. Larrañeta, A. Clark, C. Jarrahian, A. Rein-Weston, S. Lachau-Durand, N. Niemeijer, P. Williams, C. Haeck, H.O. McCarthy, D. Zehrung, R.F. Donnelly, Design, formulation and evaluation of novel dissolving microarray patches containing a long-acting rilpivirine nanosuspension, J. Control. Release 292 (2018) 119–129, https://doi.org/10.1016/j.jconrel.2018.11.002.
[80] M.T.C. Mc Crudden, E. Larrañeta, A. Clark, C. Jarrahian, A. Rein-Weston, B. Creelman, Y. Moyo, S. Lachau-Durand, N. Niemeijer, P. Williams, H. O. McCarthy, D. Zehrung, R.F. Donnelly, Design, formulation, and evaluation of novel dissolving microarray patches containing rilpivirine for intravaginal delivery, Adv. Healthc. Mater. 8 (2019) 1801510, https://doi.org/10.1002/adhm.201801510.
[81] L.K. Vora, R.F. Donnelly, E. Larrañeta, P. González-Vázquez, R.R.S. Thakur, P. R. Vavia, Novel bilayer dissolving microneedle arrays with concentrated PLGA nano-microparticles for targeted intradermal delivery: proof of concept, J. Control. Release 265 (2017) 93–101, https://doi.org/10.1016/j.jconrel.2017.10.005.
[82] Y.T. Kim, B.K. Shin, V.K. Garripelli, J.K. Kim, E. Davaa, S. Jo, J.S. Park, A thermosensitive vaginal gel formulation with HPγCD for the pH-dependent release and solubilization of amphotericin B, Eur. J. Pharm. Sci. 41 (2010) 399–406, https://doi.org/10.1016/j.ejps.2010.07.009.
[83] P. Jansook, Z. Fülöp, G.C. Ritthidej, Amphotericin B loaded solid lipid nanoparticles (SLNs) and nanostructured lipid carrier (NLCs): physicochemical and solid-solution state characterizations, Drug Dev. Ind. Pharm. 45 (2019) 560–567, https://doi.org/10.1080/03639045.2019.1569023.
[84] C. Salerno, D.A. Chiappetta, A. Arechavala, S. Gorzalczany, S.L. Scioscia, C. Bregni, Lipid-based microtubes for topical delivery of amphotericin B, Colloids Surf. B: Biointerfaces 107 (2013) 160–166, https://doi.org/10.1016/j.colsurfb.2013.02.001.
[85] B. Gebben, M.H.V. Mulder, C.A. Smolders, Thermal behavior of polytriazole films: a thermal analysis study, J. Polym. Sci. Part A Polym. Chem. 27 (1989) 3481–3494, https://doi.org/10.1002/pola.1989.080271025.
[86] Y. Tian, K. Qian, E. Jacobs, E. Amstad, D.S. Jones, L. Stella, G.P. Andrews, The investigation of flory-huggins interaction parameters for amorphous solid dispersion across the entire temperature and composition range, Pharmaceutics 11 (2019), https://doi.org/10.3390/pharmaceutics11080420.
[87] Y. Kong, J.N. Hay, The measurement of the crystallinity of polymers by DSC, Polymer (Guildf). 43 (2002) 3873–3878, https://doi.org/10.1016/S0032-3861(02)00235-5.
[88] Y. Tian, K. Qian, E. Jacobs, E. Amstad, D.S. Jones, L. Stella, G.P. Andrews, The investigation of flory-huggins interaction parameters for amorphous solid dispersion across the entire temperature and composition range, Pharmaceutics 11 (2019), https://doi.org/10.3390/pharmaceutics11080420.
[89] Y. Zu, W. Sun, X. Zhao, W. Wang, Y. Li, Y. Ge, Y. Liu, K. Wang, Preparation and characterization of amorphous amphotericin B nanoparticles for oral administration through liquid antisolvent precipitation, Eur. J. Pharm. Sci. 53 (2014) 109–117, https://doi.org/10.1016/j.ejps.2013.12.005.
[90] Y.-T. Kim, B.-K. Shin, V.K. Garripelli, J.-K. Kim, E. Davaa, S. Jo, J.-S. Park, A thermosensitive vaginal gel formulation with HPγCD for the pH-dependent release and solubilization of amphotericin B, Eur. J. Pharm. Sci. 41 (2010) 399–406, https://doi.org/10.1016/J.EJPS.2010.07.009.
[91] N. Rasenack, B.W. Müller, Micron-size drug particles: common and novel micronization techniques, Pharm. Dev. Technol. 9 (2004) 1–13, https://doi.org/10.1081/PDT-120027417.
[92] W. Yang, K.P. Johnston, R.O. Williams, Comparison of bioavailability of amorphous versus crystalline itraconazole nanoparticles via pulmonary administration in rats, Eur. J. Pharm. Biopharm. 75 (2010) 33–41, https://doi.org/10.1016/j.ejpb.2010.01.011.
[93] P. Khadka, J. Ro, H. Kim, I. Kim, J.T. Kim, H. Kim, J.M. Cho, G. Yun, J. Lee, Pharmaceutical particle technologies: an approach to improve drug solubility, dissolution and bioavailability, Asian J. Pharm. Sci. 9 (2014) 304–316, https://doi.org/10.1016/j.ajps.2014.05.005.
[94] A. Dokoumetzidis, P. Macheras, A century of dissolution research: from Noyes and Whitney to the biopharmaceutics classification system, Int. J. Pharm. 321 (2006) 1–11, https://doi.org/10.1016/j.ijpharm.2006.07.011.
[95] J.P. Jain, N. Kumar, Development of amphotericin B loaded polymersomes based on (PEG)3-PLA co-polymers: factors affecting size and in vitro evaluation, Eur. J. Pharm. Sci. 40 (2010) 456–465, https://doi.org/10.1016/j.ejps.2010.05.005.
[96] Y. Aso, S. Yoshioka, S. Kojima, Molecular mobility-based estimation of the crystallization rates of amorphous Nifedipine and phenobarbital in poly (vinylpyrrolidone) solid dispersions, J. Pharm. Sci. 93 (2004) 384–391, https://doi.org/10.1002/jps.10526.
[97] K. Qian, L. Stella, D.S. Jones, G.P. Andrews, H. Du, Y. Tian, Drug-rich phases induced by amorphous solid dispersion: arbitrary or intentional goal in oral drug delivery? Pharmaceutics. 13 (2021) 889, https://doi.org/10.3390/pharmaceutics13060889.

[98] L.G. Leanse, X.S. Goh, T. Dai, Quinine improves the fungicidal effects of antimicrobial blue light: implications for the treatment of cutaneous candidiasis, Lasers Surg. Med. 52 (2020) 569–575, https://doi.org/10.1002/lsm.23180.
[99] D.A. Sanchez, D. Schairer, C. Tuckman-Vernon, J. Chouake, A. Kutner, J. Makdisi, J.M. Friedman, J.D. Nosanchuk, A.J. Friedman, Amphotericin B releasing nanoparticle topical treatment of Candida spp. in the setting of a burn wound, Nanomedicine 10 (2014) 269–277, https://doi.org/10.1016/j.nano.2013.06.002.
[100] T. Moolakkadath, M. Aqil, A. Ahad, S.S. Imam, B. Iqbal, Y. Sultana, M. Mujeeb, Z. Iqbal, Development of transethosomes formulation for dermal fisetin delivery: Box–Behnken design, optimization, *in vitro* skin penetration, vesicles–skin interaction and dermatokinetic studies, Artif. Cells Nanomed. Biotechnol. 46 (2018) 755–765, https://doi.org/10.1080/21691401.2018.1469025.
[101] E. Larrañeta, R.E.M. Lutton, A.D. Woolfson, R.F. Donnelly, Microneedle arrays as transdermal and intradermal drug delivery systems: materials science, manufacture and commercial development, Mater. Sci. Eng. R. Rep. 104 (2016) 1–32, https://doi.org/10.1016/j.mser.2016.03.001.
[102] E. McAlister, B. Dutton, L.K. Vora, L. Zhao, A. Ripolin, D.S.Z.B.P.H. Zahari, H. L. Quinn, I.A. Tekko, A.J. Courtenay, S.A. Kelly, A.M. Rodgers, L. Steiner, G. Levin, E. Levy-Nissenbaum, N. Shterman, H.O. McCarthy, R.F. Donnelly, Directly compressed tablets: a novel drug-containing reservoir combined with hydrogel-forming microneedle arrays for transdermal drug delivery, Adv. Healthc. Mater. (2020), 2001256, https://doi.org/10.1002/adhm.202001256.
[103] T.P. Sullivan, W.H. Eaglstein, S.C. Davis, P. Mertz, The pig as a model for human wound healing, Wound Repair Regen. 9 (2001) 66–76, https://doi.org/10.1046/j.1524-475X.2001.00066.x.
[104] A. Hussain, A. Samad, S.K. Singh, M.N. Ahsan, A. Faruk, F.J. Ahmed, Enhanced stability and permeation potential of nanoemulsion containing sefsol-218 oil for topical delivery of amphotericin B, Drug Dev. Ind. Pharm. 41 (2015) 780–790, https://doi.org/10.3109/03639045.2014.902957.
[105] R.K.P. Benninger, D.W. Piston, Two-photon excitation microscopy for the study of living cells and tissues, Curr. Protoc. Cell Biol. 4 (2013), https://doi.org/10.1002/0471143030.cb0411s59. Unit.
[106] B.G. Wang, K. König, K.J. Halbhuber, Two-photon microscopy of deep intravital tissues and its merits in clinical research, J. Microsc. 238 (2010) 1–20, https://doi.org/10.1111/j.1365-2818.2009.03330.x.
[107] J.J. Torrado, R. Espada, M.P. Ballesteros, S. Torrado-Santiago, Amphotericin B formulations and drug targeting, J. Pharm. Sci. 97 (2008) 2405–2425, https://doi.org/10.1002/jps.21179.
[108] G.J. Wijnant, K. Van Bocxlaer, V. Yardley, A. Harris, S. Murdan, S.L. Croft, Relation between skin pharmacokinetics and efficacy in AmBisome treatment of murine cutaneous leishmaniasis, Antimicrob. Agents Chemother. 62 (2018), https://doi.org/10.1128/AAC.02009-17.
[109] A.H. Groll, H. Kolve, Antifungal agents: in vitro susceptibility testing, pharmacodynamics, and prospects for combination therapy, Eur. J. Clin. Microbiol. Infect. Dis. 23 (2004) 256–270, https://doi.org/10.1007/s10096-004-1108-6.
[110] A.H. Sabri, Z. Cater, P. Gurnani, J. Ogilvie, J. Segal, D.J. Scurr, M. Marlow, Intradermal delivery of imiquimod using polymeric microneedles for basal cell carcinoma, Int. J. Pharm. 589 (2020), https://doi.org/10.1016/j.ijpharm.2020.119808.
[111] A. Riezk, K. van Bocxlaer, V. Yardley, S. Murdan, S.L. Croft, Activity of amphotericin B-loaded chitosan nanoparticles against experimental cutaneous leishmaniasis, Molecules 25 (2020), https://doi.org/10.3390/molecules25174002.
[112] Y. Shadkchan, Z. Zaslavsky, E. Segal, Pharmacokinetics of amphotericin B in serum and tissues in mice treated with amphotericin B-Intralipid, Med. Mycol. 41 (2003) 15–19, https://doi.org/10.1080/mmy.41.1.15.19.
[113] K.J. Christiansen, E.M. Bernard, J.W.M. Gold, D. Armstrong, Distribution and activity of amphotericin B in humans, J. Infect. Dis. 152 (1985) 1037–1043, https://doi.org/10.1093/infdis/152.5.1037.
[114] M.R. Shirzadi, Lipsosomal amphotericin B: a review of its properties, function, and use for treatment of cutaneous leishmaniasis, Res. Rep. Trop. Med. 10 (2019) 11–18, https://doi.org/10.2147/rrtm.s200218.
[115] G. Cuddihy, E.K. Wasan, Y. Di, K.M. Wasan, The development of oral amphotericin b to treat systemic fungal and parasitic infections: has the myth been finally realized? Pharmaceutics. 11 (2019) 99, https://doi.org/10.3390/pharmaceutics11030099.
[116] D. Ellis, Amphotericin B: spectrum and resistance, J. Antimicrob. Chemother. 49 (2002) 7–10, https://doi.org/10.1093/jac/49.suppl_1.7.
[117] N.K. Copeland, N.E. Aronson, Leishmaniasis: treatment updates and clinical practice guidelines review, Curr. Opin. Infect. Dis. 28 (2015) 426–437, https://doi.org/10.1097/QCO.0000000000000194.
[118] A. Ponte-Sucre, F. Gamarro, J.C. Dujardin, M.P. Barrett, R. López-Vélez, R. García-Hernández, A.W. Pountain, R. Mwenechanya, B. Papadopoulou, Drug resistance and treatment failure in leishmaniasis: a 21st century challenge, PLoS Negl. Trop. Dis. 11 (2017), e0006052, https://doi.org/10.1371/journal.pntd.0006052.
[119] A. Chakrabarti, R. Singh, The emerging epidemiology of mould infections in developing countries, Curr. Opin. Infect. Dis. 24 (2011) 521–526, https://doi.org/10.1097/QCO.0b013e32834ab21e.